
Electronic Thesis and Dissertation Repository

2-10-2023 3:00 PM

Effects of wind turbine rotor positioning on tornado induced loads

Juan P. Lopez Ortiz, *The University of Western Ontario*

Supervisor: El Damatty, Ashraf., *The University of Western Ontario*

: Hangan, Horia., *The University of Western Ontario*

A thesis submitted in partial fulfillment of the requirements for the Master of Engineering
Science degree in Civil and Environmental Engineering

© Juan P. Lopez Ortiz 2023

Follow this and additional works at: <https://ir.lib.uwo.ca/etd>



Part of the [Other Civil and Environmental Engineering Commons](#)

Recommended Citation

Lopez Ortiz, Juan P., "Effects of wind turbine rotor positioning on tornado induced loads" (2023).
Electronic Thesis and Dissertation Repository. 9120.
<https://ir.lib.uwo.ca/etd/9120>

This Dissertation/Thesis is brought to you for free and open access by Scholarship@Western. It has been accepted for inclusion in Electronic Thesis and Dissertation Repository by an authorized administrator of Scholarship@Western. For more information, please contact wlsadmin@uwo.ca.

Abstract

This study investigates the loads induced by a large-scale tornado simulation on a horizontal axis wind turbine (HAWT) to assess the influence of three-dimensional flows with respect to the HAWT position. The loads were analyzed under two rotor operational conditions, idling and parked, at five radial distances. Subsequently, experimental validation of the numerical code HIW-TUR was conducted by evaluating the induced moments for various yaw and pitch angles. The experimental results demonstrated that the bending moment was the most important in terms of magnitude and variation with respect to the HAWT position. Furthermore, The HIW-TUR code accurately identified the magnitude and HAWT configuration that leads to the maximum mean moments induced by the tornado. It was proved that by varying the yaw angle of the rotor plane and blade orientation to parallel to the tornado tangential component, the overall loads could be reduced to the minimum values.

Keywords

Tornado, Wind Turbine, Experimental Test, WindEEE, Loads, Experimental Validation,

Summary for Lay Audience

The transition to renewable energies driven to reduce fossil fuels emissions has promoted an accelerated growth in wind turbine rotors size and wind turbine expansion in high-density wind regions. The combination of new larger wind turbines and exposure to localized high-intensity winds developed in those high-density wind regions have created scientific concerns to study the effects of the induced unconventional three-dimensional tornado flow loads acting on wind turbines and the effects of the tornado location with respect to the wind turbine.

This thesis conducted an experimental simulation of a large-scale tornado acting on a wind turbine to examine the variation of the loading effects with respect to different wind turbine location, orientation, and operational condition and identify those configurations that could lead to structural failure and those that could reduce the loads and help to protect the wind turbine system. Additionally, the results from the experimental tests were compared to numerical results to validate an in-house developed code. This numerical code, once validated, could expand the number of variables to study and identify the loads in specific wind turbine elements.

Co-Authorship Statement

This thesis has been prepared as an integrated-article format stipulated by the Faculty of Graduate Studies at Western University. Chapter 2 and Chapter 3 are formatted as a journal articles.

Chapter two is a journal article submitted to Wind and Structures Journal, under co-authorship of Juan P. Lopez, Horia Hangan, and Ashraf El Damatty. In this chapter the original data of the tornado wind field was provided by Ashrafi. et al. The design of the experimental tests, analysis work on data and draft writing was carried out by the candidate under supervision of professors Horia Hangan and Ashraf El Damatty.

Chapter three will be submitted as a journal article, under co-authorship of Juan P. Lopez, Horia Hangan, Ashraf El Damatty, and Mohamed AbuGazia. In this chapter the numerical code was developed by Mohamed AbuGazia. The analysis work on data and models, draft writing and edition was carried out by the candidate under supervision of professors Horia Hangan and Ashraf El Damatty.

Acknowledgments

I would like to express my sincere gratitude to my supervisors Prof. El Damatty and Prof. Horia Hangan, for providing me with the opportunity to work with first-class researchers and unique facilities in wind engineering. I will always be grateful for their patience and overwhelming support throughout this research experience.

I would like to thank all my friends and colleagues in the Civil and Environmental Engineering department who accompanied me throughout these challenging years, especially my friends Gabriel Narancio, Mostafa Hamed and Mohamed AbuGazia.

I would like to acknowledge the Mexican National Council for Science and Technology (CONACYT) for the financial support all over this research.

Lastly, I would like to thank my parents, Rosa and Jose; my brothers and their families, Luis and Rafael; and my wife and daughter, Emma and Ofelia.

Table of Contents

Abstract.....	i
Summary for Lay Audience.....	ii
Co-Authorship Statement.....	iii
Acknowledgments.....	iv
Table of Contents.....	v
List of Tables.....	viii
List of Figures.....	ix
Chapter 1.....	1
1 Introduction.....	1
1.1 Wind energy expansion and consequence.....	1
1.2 Tornadoes.....	6
1.3 Horizontal Axis Wind Turbines.....	7
1.4 Research objectives.....	10
1.5 Motivation and contribution.....	11
1.6 Thesis outline.....	12
1.7 References.....	13
Chapter 2.....	15
2 Experimental study of the loads induced by a large-scale tornado simulation on a HAWT model.....	15
2.1 Introduction.....	15
2.2 Tornado-induced loads on structures.....	17
2.2.1 Tornado characteristics.....	17
2.2.2 Tornado-induced loads on buildings.....	18

2.2.3	Tornado-induced loads on HAWT.....	19
2.3	Methodology	20
2.3.1	The WindEEE Dome	20
2.3.2	Large-scale Mode B Tornado	21
2.3.3	Wind turbine model	22
2.3.4	Experimental setup.....	23
2.3.5	Uncertainty analysis.....	27
2.4	Results and discussion	28
2.4.1	TLV-induced moment.....	28
2.4.2	Lateral and torsional moment dependency on the three-dimensional TLV flow	33
2.4.3	Preliminary comparison between uniform, ABL and tornado induced bending moments	35
2.4.4	Full-scale comparison of experimental and numerical induced maximum moments.....	37
2.5	Conclusions.....	39
2.6	References.....	40
Chapter 3	45
3	Experimental validation of a numerical model for tornado-induced loads on a HAWT for a variety of pitch and yaw angles	45
3.1	Introduction.....	45
3.2	Experimental tornado-induced loads on a HAWT.....	48
3.2.1	Large-scale tornado characteristics.....	49
3.2.2	Wind turbine details	52
3.2.3	Experimental tornado-induced loads on a HAWT.....	53
3.3	Experimental HIW-TUR validation.....	53
3.3.1	Description of the numerical code	54

3.3.2	Validation discussion	58
3.4	Case study	59
3.4.1	Case study discussion	61
3.5	Conclusions.....	66
3.6	References.....	66
Chapter 4	70
4	Conclusion	70
4.1	Recommendation and future work.....	71
Curriculum Vitae	72

List of Tables

Table 1 Comparison of F-Scale and EF-Scale wind speeds	7
Table 2 Experimental test cases	25

List of Figures

Figure 1 Vertical-axis windmill for milling grain, Afghanistan. Deutsches Museum (Hau, 2013).	1
Figure 2 World renewable electricity capacity, 2010-2021 (IRENA and ILO, 2022).	2
Figure 3 Average turbine nameplate capacity, hub height, and rotor diameter for land-based wind projects in the United States (EERE, 2022).....	4
Figure 4 Offshore wind turbine rotor size of current projects, *projects in development, and **projected size (IEA, 2019)	5
Figure 5 Wind turbine developments and tornado risk in North America	5
Figure 6 Effect of aerodynamic, gravitational, and inertial loads of the rotor of HAWT (Hau, 2013)	9
Figure 7 Experimental setup scheme	24
Figure 8 Small scale horizontal axis wind turbine.....	24
Figure 9 Position of the wind turbine in the WinDEE Dome test chamber	26
Figure 10 Force-balance and light sensor location in the wind turbine	27
Figure 11 Mean moments at the tower base on the idling wind turbine at five radial distances from the tornado center	29
Figure 12 Tangential velocity contours of Mode B Tornado (m/s)	29
Figure 13 Mean bending moments and TSR for idling and parked conditions	31
Figure 14 Power spectral density of the bending moments	33
Figure 15 Normalized torsional moment	33

Figure 16 Normalized lateral moment	34
Figure 17 Radial (Left) and axial (Right) vertical velocity profiles for different radii	35
Figure 18 Normalized wind vertical velocity profiles	36
Figure 19 Bending moment coefficient comparison for an ABL, uniform, and tornado flow	37
Figure 20 Experimental and numerical bending moment at the tower base. (I) Idling, (P) Parked, and (O) Operating	38
Figure 21 Scheme with the dimensions of the small-scale HAWT and the radial distance variable with respect to the tornado core center	49
Figure 22 velocity component contours of Mode B Tornado: U_t (top), U_r (middle), U_a (bottom).....	51
Figure 23 Twist angle and chord length distribution along the blade.....	52
Figure 24 Force diagram of an airfoil section (i).....	55
Figure 25 Variable twist angle with respect to the blade length L	56
Figure 26 Experimental and numerical bending moment at the tower-base of the small- scale HAWT at five normalized distances	58
Figure 27 Scheme of the HAWT orientation with the variables r and δ	59
Figure 28 Vertical profiles of U_t , U_r , and U_a of the CFD simulated tornado	60
Figure 29 U_t vertical profiles of the Mode B tornado and CFD simulation at r_{max}	61
Figure 30 Overall moment on the small-scale HAWT varying delta angle and radial position.....	62

Figure 31 Comparison of the bending moment at the tower base for a HAWT with constant pitch angle and twisted blades 63

Figure 32 Flap-wise moment on the blades of the HAWT at different tornado approaching angle 64

Figure 33 Flap-wise moment on the blades varying the pitch and tornado approaching angle 64

Figure 34 Moment at the base of the tower of a HAWT varying the pitch and approaching tornado angles 65

Chapter 1

1 Introduction

1.1 Wind energy expansion and consequence

Wind energy is the kinetic energy in the air motion used to generate mechanical power. In the early attempts of harvesting the energy available from the wind, the mechanical power produced by wind-based machines was utilized mainly for grinding grain or pumping water. One of the most antique pieces of evidence of use of wind energy was found in the Persian-Afghan region of Seistan dated in the year 644 A.D. It appeared to be a wind machine with a vertical rotor axis similar to primitive windmills located in Afghanistan (Figure 1). However, information about the origins of wind energy machines is not clear, and there are speculations about ancient wind energy use in Egypt, Greece, and China (Hau, 2013).



Figure 1 Vertical-axis windmill for milling grain, Afghanistan. Deutsches Museum (Hau, 2013).

Nowadays, wind turbines employ wind energy to rotate rotor blades by converting the kinetic energy into rotational mechanical power, which is transferred to an electrical generator to produce electricity. Technological advances produced throughout the 20th century allowed to improve the cost-efficiency of wind turbines and transform them into an affordable and reliable clean energy alternative. Additionally, the transition to renewable energies to address the climate crisis and the concerns associated with greenhouse gas emissions delivered by fossil fuels have promoted an accelerated growth in this industry. This push has driven a rapid spread of new wind turbine developments and electrical shares worldwide. Just in the past decade, 2010-2021, the installed capacity in the world of energy from all types of renewable sources increased by 130% (IRENA & ILO, 2022). According to the International Renewable Energy Agency Market report 2022, wind energy represented a four-fold increase in the same period (Figure 2).

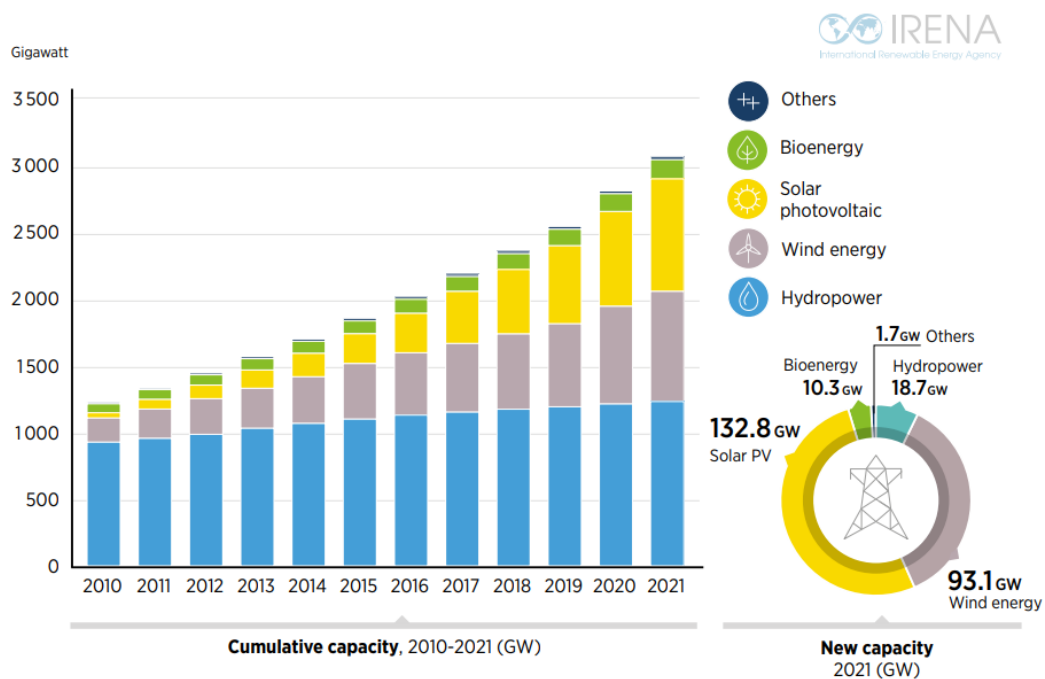


Figure 2 World renewable electricity capacity, 2010-2021 (IRENA and ILO, 2022).

Furthermore, policy support from international organizations and national strategy plans to adopt wind energy as an alternative to renew or expand their power necessities estimate a continuous growing with an accelerated pace in the next 20 years. Among several initiatives to embrace green technologies, the 1.5°C Scenario outlined in the 2021

World Energy Transitions Outlook (WETO) envisioned the endorse of wind energy adoption to meet the 1.5°C Paris climate goal. Therefore, a wind power generation goal of about 7 900 TWh in 2030 was established to accomplish zero contaminant emission in 2050. This requires new wind energy installed capacity to expand 18% per year towards 2030. (IRENA, 2022).

One major consequence of wind energy expansion is the increment of wind turbine dimensions. As wind energy is proportional to the wind turbine rotor size, industry pushes for wind turbines with larger swept area in order to increase the profitability. Larger rotors allow to capture more wind and produce more electricity. Consequently, wind turbine rotor areas have increased around 600% from 1998 to 2021. However, rotor scaling has been especially significant in the last decade. According to the Energy Efficiency and Renewable Energy Office (EERE), the average hub height of wind turbines installed in 2021 was 93.9 meters, 4% larger than in 2020 and up 66% since 1998 (EERE, 2022). The average rotor diameter in 2021 was 127.5 meters, 2% larger than in 2020 and up 164% since 1998 (Figure 3). However, wind turbines located on the sea, or offshore wind turbines, experienced the largest change in size due to the absence of obstacles such as human settlements, natural reserves, or farmlands. Moreover, wind developments located on the sea experience higher mean annual wind energy density, or the wind energy per unit of area normal to the wind direction, and steady velocities due to lower roughness factors of the sea surface. For instance, it is projected that a wind turbine with 260 meters in diameter could be working in 2030 (Figure 4), this is nearly the double of the average rotor size of present land-based wind turbines (IEA, 2019).

A second important consequence of wind energy expansion is the increase in number of wind turbine systems. As the kinetic energy available in the wind varies with the cube of the wind velocity, it is essential to place these new developments in a suitable site with good mean annual wind energy density. In North America, North-Western and North-Eastern coasts are appropriate for wind turbine developments. Additionally, there are regions with high wind velocities in the Great Plains from Texas in the South to Nebraska in the North of the United States, including the South part of the provinces of Saskatchewan, Manitoba, and Ontario in Canada. New utility-scale wind turbines have

been installed in this region, and most of the operating land-based wind farms in North America are located in this territory or in the vicinity. However, land areas evaluated with strong velocity winds are usually also prone to localized High Intensity Winds (HIW) produced in thunderstorms, such as downbursts and tornadoes, which possess dangerous wind fields attributes different to storms produced by tropical cyclones. Unfortunately, most of the wind turbine developments installed in North America observed in Figure 5 are located in areas of influence of the so-called Tornado Alley, which is an area between the Appalachian Mountains and the Rocky Mountains with historical HIW events, especially tornado occurrences.

The combination of new wind turbines with rotor diameters larger than 200 meters and the increased of wind turbine systems presence in high-density wind regions prone to develop HIW events such as tornadoes have created, from the point of view of wind and structural engineering, serious concerns about the structural safety of wind turbines due to the three-dimensional tornado flow loads.

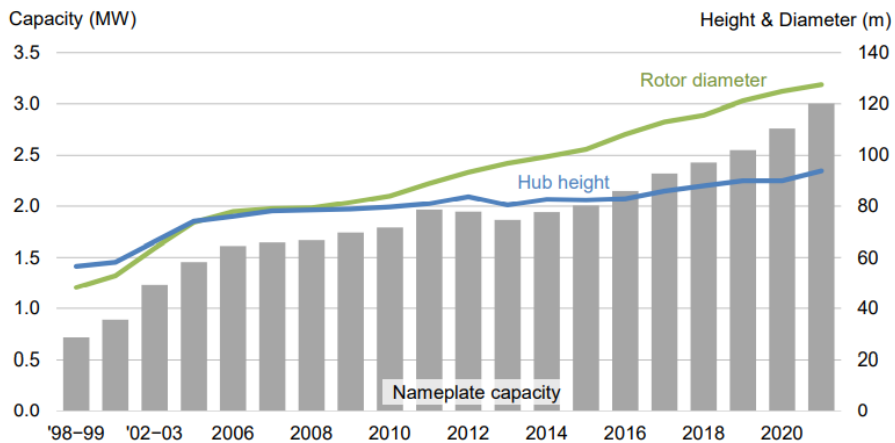


Figure 3 Average turbine nameplate capacity, hub height, and rotor diameter for land-based wind projects in the United States (EERE, 2022)

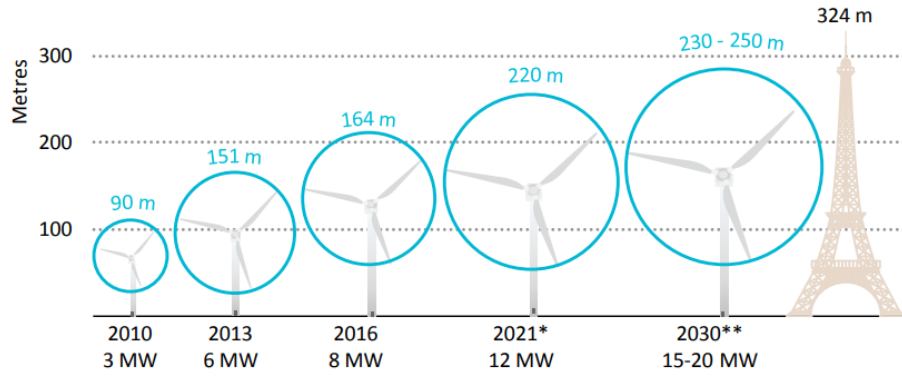


Figure 4 Offshore wind turbine rotor size of current projects, *projects in development, and **projected size (IEA, 2019)

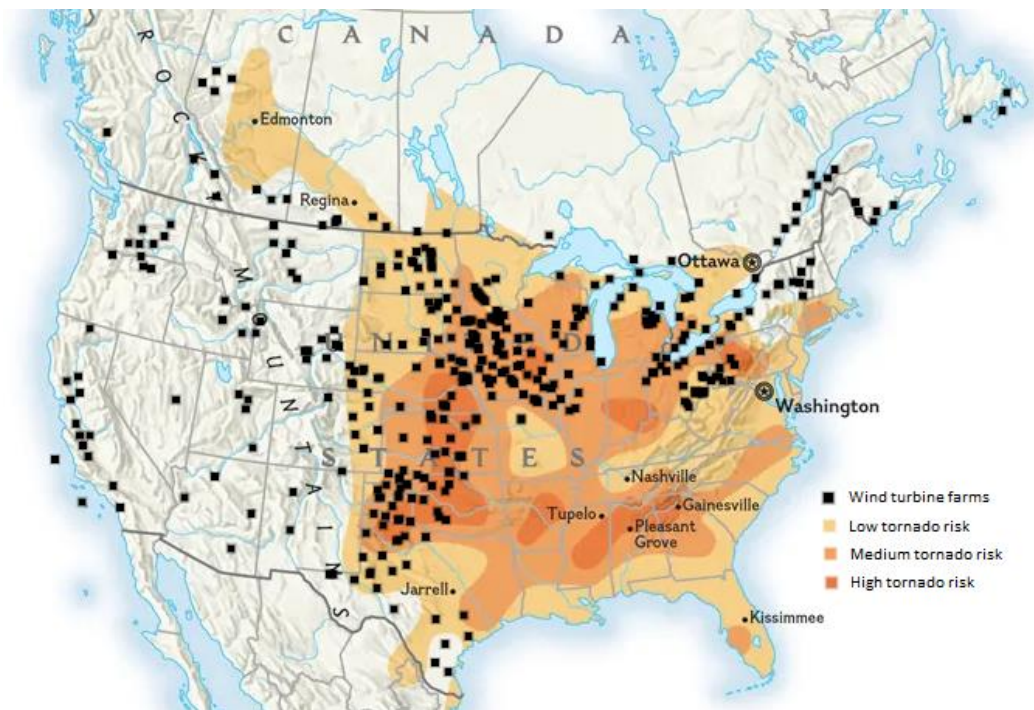


Figure 5 Wind turbine developments and tornado risk in North America

1.2 Tornadoes

The American Meteorological Society (AMS) defined tornado as “a rapidly rotating column of air extending vertically from the surface to the base of a cumuliform cloud, often with near-surface circulating debris/dust when over land or spray when over water.” (AMS, 2022). Tornadoes are one of the most hazardous atmospheric events in nature and effects on structures can be more damaging than ordinary tropical cyclonic storms.

The exact process of tornado creation, or tornadogenesis, is not fully clear yet, but most dangerous tornadoes are related to the formation of mesocyclones due to temperature differences. Theories suggest that tornadogenesis develop from supercell thunderstorms, which usually builds when one of the convective single cells expands and consumes other cells in a multicell thunderstorm. A strong vertical wind shear causes a horizontally rotating cylinder of air, and the updraft lifts the rotating cylinder within the supercell. Afterwards, the vortex, or funnel, of air contracts and intensify the swirling velocity due to the principle of the conservation of momentum. As air converges toward the axis of rotation, mass conservation would require it also move upward causing further contraction of the radii of rotation leading to a stronger vortex and the formation of a tornado (Markowski & Richardson, 2014).

In order to know the wind speed velocity and statistics, tornadoes were commonly categorized in the Fujita (F) scale based on the destruction left behind by the tornado main path (Fujita, 1971). However, the F-scale based the classification only in the damage indicator with no correlation between the damage and wind speed information, leading to inconsistent classification and overestimation of wind speeds. At present, a new Enhanced Fujita scale (EF) classifies tornadoes by their destructive potential considering 28 damage indicators, including the type and quality of structures (WSEC, 2004). EF-scale consist of 5 categories ranging from EF0 to EF5 that represent estimated 3-second gusts from 105 km/h to over 321 km/h (Table 1).

Table 1 Comparison of F-Scale and EF-Scale wind speeds

F/EF Rating	F-Scale Wind Speed Rounded to 10 km/h	EF-Scale Wind Speed Rounded to 5 km/h
0	60-110	90-130
1	120-170	135-175
2	180-240	180-220
3	250-320	225-265
4	330-410	270-310
5	420-510	315 or more

From an engineering perspective, tornadoes are three-dimensional wind fields with tangential (U_t), radial (U_r), and vertical (U_a) velocity components. The vertical shear velocity distribution of their velocity components differs from those from Atmospheric Boundary Layers (ABL) with a peak velocity near the ground, in particular, the tangential velocity component, which is the most important in velocity magnitude and variation. Moreover, uncertainties related to the translational movement, including wandering displacements of the core center, represents higher risks to aerodynamic structures with safety control strategies, such as wind turbines. Ward (1972) classified the tornado wind field into three regions:

- The outer region or confluences is characterized by a radial convergence. The axial velocity component is generally restrained, and the radial velocity component inflow dominate the wind field.
- The central or convergence region is characterized by significant effects of the axial velocity component and the tangential velocity component. In particular, the velocity tangential component, which possess a strong angular momentum and a high velocity peak near the ground surface.
- The convection region is a nearly uniform horizontal pressure field that provides the vortex with an upper boundary condition.

1.3 Horizontal Axis Wind Turbines

A wind turbine is a device that convert the kinetic energy in the wind into electricity by generating a rotational movement from the rotor blades induced by aerodynamic forces. The wind flows across the airfoil sectional shape of the blades to generate lift and drag

forces. The resultant force causes the rotor spin around a central hub connected to an electrical generator to transform the mechanical energy into electrical power.

Wind turbines can be classified by their aerodynamic function when the wind turbine generates movement by the drag force or by the lift force, and by the orientation of the axis of rotation of the wind rotor in vertical axis wind turbines (VAWT) and horizontal axis wind turbines (HAWT). However, HAWT devices have demonstrated several advantages over all other designs, converting them as the wind energy turbine standard for utility-scale wind farms. For instance, the rotor speed and power output can be controlled by varying the rotor blade pitch angle, the aerodynamic lift can achieve higher efficiency than drag force devices, and the wind turbine rotor can be oriented by a yaw movement to increase the swept area.

Besides energy efficiency, another important aspect of wind turbine designs is the structural safety. As a big slender structure, wind turbines elements are subjected to different source and types of loads. These loads are even more complex due to the aerodynamic effects of the wind turbine blades and cycling movements of the rotor. The structural design is lead mainly by three main aspects: The breaking strength point, the fatigue resistance, and the stiffness of components. And theses structural aspects must be evaluated by all forces acting on the rotor attributable to aerodynamic, gravitational, and inertial forces. All the effects generated by the different forces acting on a wind turbine can be summarized in Figure 6.






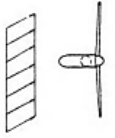
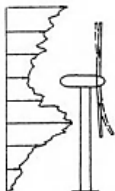
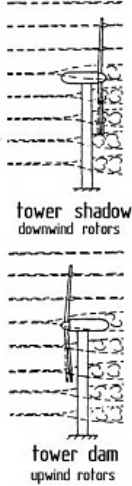
		Aerodynamic forces	Inertial and gravity forces
steady loads		 steady mean wind speed	 centrifugal forces
	cyclic loads	 vertical wind shear	 gravity forces  gyroscopic forces
		 cross winds yaw angle	
non-cyclic loads	 wind turbulence	 tower shadow downwind rotors tower dam upwind rotors	

Figure 6 Effect of aerodynamic, gravitational, and inertial loads of the rotor of HAWT (Hau, 2013)

One more significant component to understand the aerodynamic loading effects on wind turbine rotors is the airfoil shape of HAWT blades. An airfoil is a shape designed to produce a lift force generated by the movement of the air crossing the airfoil section. The geometrical shape of an airfoil can vary along the airfoil chord, symmetry with respect to the chord or the wider of the camber. However, the general silhouette is a drop-like shape. The drop-like shape of the airfoil accelerates the flow in the upper surface with

bigger convexity, this produces a lower pressure on the upper part resulting in a suction or lifting force. The lift and drag forces generated by airfoils depend on the fluid density, velocity of the flow, the airfoil shape, dimension, and orientation with respect to the oncoming flow. A convenient way to employ the lift and drag forces is the use of dimensionless coefficients by using the Lift coefficient and Drag coefficient (Cengel & Cimbala, 2018) defined by:

$$C_D = \frac{F_D}{\frac{1}{2}\rho U^2 A} \quad (1)$$

$$C_L = \frac{F_L}{\frac{1}{2}\rho U^2 A} \quad (2)$$

Where F_D and F_L are the lift and drag forces, A is the airfoil reference area, ρ is the fluid density and U is the velocity of the flow. The information of the C_D and C_L values varying the blade orientation with respect to the oncoming wind or the resultant velocity component for various velocity components in the wind field. These coefficients are an important foundation for several numerical and analytical theories to calculate the forces acting on wind turbines rotors, such as the numerical procedure described and used in Chapter 3.

1.4 Research objectives

General objective:

- Assess the variation of the straining actions acting on an HAWT with respect to the tornado position and the wind turbine rotor operation condition to identify the configuration that could lead to structural failure and the configuration that could reduce the loads in the overall system and individual elements.

The general objective can be subdivided into several particular objectives:

- Compare the straining actions acting on HAWT arising from tornadoes and those from ABL at similar wind speeds at the hub level.

- Compare the straining actions produced by tornadoes and the corresponding values calculated by the Design Load Case (DLC) 1.3 of the International Electrotechnical Commission (IEC) standard 61400-1 (IEC, 2007) for ABL flows using the extreme turbulence model (ETM).
- Validate experimentally a developed numerical model comparing the tornado-induced bending moment obtained in the experimental measurements on a wind turbine under various locations.
- Analyze a HAWT using the developed numerical model to identify the tornado location that leads to the peak straining actions on the tower and blades for a variety of yaw and pitch angles.
- Determine the optimum pitch angle that leads to minimum straining actions on both the blades and the tower given the uncertainty associated with the tornado location.

1.5 Motivation and contribution

Experimental studies regarding tornado induced loads acting on wind turbines are limited in literature due to the complexity of tornado reproduction in laboratory scales and challenging field measurements due to the uncertainty associated to the tornado formation and short duration of the event. Although, several numerical and experimental studies have been performed involving wind turbines and synoptic winds interaction (Dimitrov et al., 2015; Tian et al., 2019; Santo et al., 2019; Shirzadeh et al., 2020), Only a few limited numerical studies have been performed regard tornado-induced loads acting on wind turbines. For example, it has been demonstrated that the higher moment acting on the HAWT could be produced on different elements of wind turbines such as rotor blades, rotor disk, and tower, and it can be induced by different tornado approaching directions (Campagnolo & Biegle, 2019). Furthermore, the maximum moments acting on the wind turbine blades can be induced at different pitch angles and rotor orientations depending on the tornado location (AbuGazia et al., 2020). However, numerical studies could be deficient in including the resonant component and dynamic effects of complex tornado wind fields.

This comprehensive experimental study of proper scaled tornado-induced loads on wind turbines can provide valuable knowledge concerning wind turbine loading effects for several wind turbine configurations, rotor orientations, wind turbine positions, rotor conditions, and blades orientations. Furthermore, an experimental validation of a numerical method can improve the accuracy of the loads acting on wind turbines by non-conventional winds, expanding the number of case studies limited by time and cost in experimental research.

The results obtained by this research will help to improve the structural safety of wind turbines through control strategies during tornadoes that can reduce the loads acting on the wind turbine elements due to inappropriate wind turbine positioning. Future work could lead to improve loads predictions models used in international safety standards and design codes.

1.6 Thesis outline

In addition to the introduction of the thesis content redacted in chapter 1, chapter 2, formatted as a journal article, details the procedures, analysis, and results of an experimental study of the loads induced by a tornado-like vortex acting on a HAWT, and their loading effects on the wind turbine varying the position with respect to the tornado center and the rotor operational condition. Chapter 3 details the experimental validation of the numerical code HIW-TUR by evaluating the tornado-induced loads obtained in the experimental tests described in chapter 2 with the numerical results. Additionally, a case study is included in order to evaluate a wider amount of position and orientation of the wind turbine with respect to the tornado effects on the induced loads acting on the wind turbine system and on the rotor blades.

Finally in chapter 4, general conclusions and recommendations for future work are summarized.

1.7 References

- AbuGazia, M., El Damatty, A., Dai, K., Lu, W., & Ibrahim, A. (2020). Numerical model for analysis of wind turbines under tornadoes. *Engineering structures*, 223, 111157. <https://doi.org/10.1016/j.engstruct.2020.111157>
- American Meteorological Society (AMS). (2022). Tornado. Glossary of Meteorology. <https://glossary.ametsoc.org/wiki/tornado>
- Campagnolo, F., & Biegle, H. (2019). Numerical study of the loads induced by tornadoes on a 3.5 MW wind turbine. *Research Report No. 1*; Technische Universität München, Munich, Germany.
- Cengel, Y. A., & Cimbala, J.M. (2018). *Fluid Mechanics fundamental and application fourth edition*. McGraw Hill education.
- Dimitrov, N., Natarajan, A., & Kelly, M. (2015). Model of wind shear conditional on turbulence and its impact on wind turbine loads. *Wind Energy*, 18, 1917-1931. <https://doi.org/10.1002/we.1797>
- Energy Efficiency and Renewable Energy (EERE). (2022). *Land-based wind market report: 2022*. Office of Energy Efficiency and Renewable Energy.
- Fujita, T. T. (1971). A proposed characterization of tornadoes and hurricanes by area and intensity. *Satellite & Mesometeorology Research Project (SMRP) Paper 91*, 42. <https://ntrs.nasa.gov/citations/19720008829>
- Hau, E. (2013). *Wind turbines: fundamentals, technologies, application, economics*. Springer.
- International Energy Agency (IEA). (2019). *Offshore wind outlook 2019*.
- International Electrotechnical Commission (IEC). (2007). *Wind turbines part 1: design requirements IEC-61400-1*.

- International Renewable Energy Agency (IRENA). (2022). *World energy transitions outlook 2022: 1.5°C pathway*.
- International Renewable Energy Agency (IRENA), & International Labour Organization (ILO). (2022). *Renewable energy and jobs: Annual review 2022*.
- Markowski, P. M., & Richardson, Y. P. (2014). The Influence of Environmental Low-Level Shear and Cold Pools on Tornadogenesis: Insights from Idealized Simulations. *Journal of the Atmospheric Sciences*, 71(1), 243-275.
<https://doi.org/10.1175/JAS-D-13-0159.1>
- Santo, G., Peeters, M., Paepegem, W., & Degroote, J., (2019). Dynamic load and stress analysis of a large horizontal axis wind turbine using full scale fluid-structure interaction simulation. *Renewable Energy*, 140, 212-226.
<https://doi.org/10.1016/j.renene.2019.03.053>
- Shirzadeh, K., Hangan, H., Crawford, C., & Tari, P.H. (2020). Investigating the loads and performance of a model horizontal axis wind turbine under IEC extreme operational conditions. *Wind Energy Science*, 6, 477-489.
<https://doi.org/10.5194/wes-6-477-2021>
- Tian, W., Ozbay, A., & Hu, H. (2019). A wind tunnel study of wind loads on a model wind turbine in atmospheric boundary layer winds. *Journal of Fluids and Structures*, 85, 17-26. <https://doi.org/10.1016/j.jfluidstructs.2018.12.003>
- Ward, N.B. (1972). The exploration of certain features of tornado dynamics using a laboratory model. *J. Atmos. Sci.*, 29, 1194-1204. [https://doi.org/10.1175/1520-0469\(1972\)029<1194:TEOCFO>2.0.CO;2](https://doi.org/10.1175/1520-0469(1972)029<1194:TEOCFO>2.0.CO;2)
- Wind Science and Engineering Center (WSEC). (2004). A recommendation for an Enhanced Fujita scale (EF-Scale). The National Weather Service.

Chapter 2

2 Experimental study of the loads induced by a large-scale tornado simulation on a HAWT model

As wind turbine rotors increase, the overall loads and dynamic response become an important issue. This problem is augmented by the exposure of wind turbines to severe atmospheric events with unconventional flows such as tornadoes, which need specific designs not included in standards and codes at present. An experimental study was conducted to analyze the loads induced by a tornado-like vortex (TLV) on horizontal-axis wind turbines (HAWT). A large-scale tornado simulation developed in The Wind Engineering, Energy and Environment (WindEEE) Dome at Western University in Canada, the so-called Mode B Tornado, was employed as the TLV flow acting on a rigid wind turbine model under two rotor operational conditions (idling and parked) for five radial distances. It was observed that the overall forces and moments depend on the location and orientation of the wind turbine system with respect to the tornado vortex center, as TLV are three-dimensional flows with velocity gradients in the radial, vertical, and tangential direction. The mean bending moment at the tower base was the most important in terms of magnitude and variation in relation to the position of the HAWT with respect to the core radius of the tornado, and it was highly dependent on the rotor Tip Speed Ratio (TSR).

2.1 Introduction

The continuous development of more efficient wind turbines with relatively lower-cost energy production and higher capacity has made wind energy the fastest-growing energy source in the world (IRENA, 2019). According to the International Renewable Energy Agency, the global installed wind capacity has increased by a factor of 75 in the last two decades, and new large-scale wind turbine installations are expected to continue growing (Wiser & Bolinger, 2019).

In order to maximize the wind farms profitability, the diameter of wind turbine rotors has been continuously increasing with the purpose to extract more of the kinetic energy

available in the wind. As a result of the increase in the size of wind turbine rotors, the loads produced by the driving torque, the thrust force, and the gravitational weights of the wind turbine elements can generate higher simultaneous loads and dangerous cumulative effects than before. For horizontal-axis wind turbines (HAWT), these loads are complex due to the alternating loads of the rotor blades generated by gravitational forces in each rotor revolution, producing tensile and pressure forces (Hau, 2013). Inevitably, large wind turbines are elastic structures, and according to the simple beam theory, increasing the length of the blades will cause more flexibility and dynamic stresses due to wind loads.

In general, wind turbines are designed to extract energy and withstand high-speed winds produced by Atmospheric Boundary Layer (ABL) flows. International standards, such as The International Electrotechnical Commission 61400-1 (IEC, 2007), prescribe operating scenarios, and possible malfunctions of wind turbines under the action of specific wind loads described in design load cases (DLC) with the purpose to ensure the structural safety of the wind turbines. However, these DLCs are deterministic and defined only for ABL flows. Therefore, they exclude events related to thunderstorms such as downbursts and tornadoes, which own unconventional wind profiles (Fujita, 1981). Tornadoes in particular are considered the most hazardous atmospheric phenomena characterized by three-dimensional winds with significant tangential and vertical velocity components that produce substantially different loads compared to ABL flows (Haan et al., 2010). Tornado-induced loads are presumed to lead to structural failures in wind turbines due to their high-speed winds, high turbulence intensity, and particular three-dimensional loading effects, hence specific evaluation scenarios in codes should be required. However, the randomness and short life of tornadoes complicate the availability of wind turbine-tornado interaction field data, while at the same time physical reproduction in laboratory is limited by the required spatial resolution.

Unlike the aerodynamic loads on wind turbines induced by ABL flows that have been extensively studied experimentally and analytically in the past, there is a literature gap concerning the wind turbine-tornado interaction. A comprehensive study of proper scaled tornado-induced loads on wind turbines can improve loads prediction models,

international standards, as well as wind turbine control strategies during tornadoes, and consequentially reduce operational and structural failures in wind turbines.

This study is the first experimental program conducted under a large-scale simulated tornado for HAWTs motivated to address the literature gap concerning wind turbines-tornadoes interaction. The main objective of this research is to assess the variation of the straining actions acting on an HAWT with respect to the tornado position and the wind turbine rotor operation condition. This is in addition to the two following secondary objectives: 1) compare between the straining actions acting on HAWT arising from tornadoes and those from ABL at similar wind speeds at the hub level, and 2) compare the straining actions produced by tornadoes and the corresponding values calculated by the DLC 1.3 IEC standard 61400-1 (IEC, 2007) for ABL flows using the extreme turbulence model (ETM).

2.2 Tornado-induced loads on structures

2.2.1 Tornado characteristics

Tornadoes are vortices of rising air with significant rotational, radial, and vertical velocity components in the core region (tangential (U_t), radial (U_r), and vertical (U_a)). They form from strong circulating flows that develop beneath supercell thunderstorms when cold and dry air meets warm moist tropical air. Tornadoes can be classified by their destructive potential adopting the Enhanced Fujita scale (EF) with categories ranging from EF0 to EF5 that represent estimated 3-second gusts from 105 km/h to over 321 km/h (WSEC, 2004).

Field data from tornadoes can be obtained by using Doppler radars, but this method is limited to heights generally above 30 meters above the surface by the presence of obstacles and terrain (Refan et al., 2017). Therefore, experimental reproduction is the best source for precise tornado-induced loads data. However, the proper kinematic and dynamic scaling is a challenge for laboratory simulations due to the size and velocities reached by tornadoes in nature. Three main governing non-dimensional parameters have been defined by Lewellen (1962) and Davies-Jones (1973) to characterize TLV in a

laboratory setting: the aspect ratio (a) between the inflow height and the updraft radius, the swirl ratio (S), the ratio of the tangential velocity to the radial velocity at the inflow region, and the Radial Reynolds Number (Re_r). However, S is the dominant parameter (Church et al., 1979), and the radial variation of mean tangential velocities and surface pressures are independent for $Re_r > 4.5 \cdot 10^4$ even though Re_r in real tornadoes is generally many orders of magnitude larger than in simulated tornado-like vortices (Refan & Hangan, 2018).

2.2.2 Tornado-induced loads on buildings

Several studies have demonstrated the differences in pressure on building surfaces by tornadoes and ABL-induced loads. Chang (1971) demonstrated that a cubic model presented suction and dynamics pressures simultaneously. Jischke and Light (1983) determined that those pressures were due to the addition of the swirl component presented in tornadoes. Furthermore, the peak tornado-induced loads were greater than those caused by straight-line ABL flows with the same wind speeds. Sarkar et al. (2008) found that the peak loads and moments were greater by a factor of 1.5. Mishra et al. (2008) demonstrated that the mean surface pressures on small buildings were 3–5 times higher in TLV than in straight ABL flows. These higher pressures were not only caused by high-speed winds, but also by the overall suction produced by tornadoes. Additionally, the pressure distribution on the building surfaces were different from ABL flows in magnitude, the number of surfaces, and locations with positive and negative values. Even though, HAWTs do not display large surfaces susceptible to high pressure differentials, the three-dimensional flow could generate different loading effects on the wind turbine elements. Similar to microburst-like winds and unlike straight-line ABL flows, the acting loads depend on the location and orientation of the structure with respect to the tornado vortex center. Sarkar and Razavi (2018) showed that the peak uplift increased when a structure is located on the tornado main path and decreases at locations far from the tornado main path.

2.2.3 Tornado-induced loads on HAWT

Due to the complexity in the laboratory reproduction of wind turbine–tornado interaction, only a few limited numerical studies have been developed. The Wind Energy Institute of the Technische Universität München (TUM) conducted a numerical study of loads induced by tornadoes on a 3.35 MW HAWT using the velocity field data from the Mode B Tornado reproduced in the WinDEE Dome and the advanced aero-servo-elasticity tool Cp-Lambda (Bortolotti et al., 2016). In this report, Campagnolo and Biegle (2019) demonstrated that the loads induced by tornadoes could drive the design of the tower and main shaft components because they were higher than those included by the DLCs contained in the IEC 61400-1. However, the ultimate loads acting on the rotor blades could already be included in ABL flows specified by the IEC 61400-1, DLC 1.3 (Extreme Turbulence Model). Although, this result could be different in the case of a stronger tornado. The highest induced load was observed when the tornado was approaching the HAWT from a direction angle of 250° and the wind turbine was at a radial distance of 80 m from the center of the vortex. In general, the highest absolute moments on blades, rotor and tower were showed from different approaching directions of the TLV. For instance, the highest torsional moment on the blade root and the tower base were induced when the TLV approached the HAWT from a direction angle of 45° and at a radial distance of 40 m. However, the highest absolute value of the flap-wise moment on the blade root was showed from a direction angle of 220° .

AbuGazia et al. (2020) identified the location of the peak forces exerted by the three-dimensional winds of a stationary TLV acting from several positions around a wind turbine by using a built-in-house numerical model. It was found that the minimum straining actions on the blades occurred when the pitch angle of the blades was set at 60° , and the minimum straining actions on the tower took place when the pitch angles were set at 15° . Also, a comparison between the results of their simulations and the extreme wind load scenarios included in the IEC 61400-1 standard, showed that the predicted straining actions produced by the simulated EF2 tornado were higher than those included in the standard.

2.3 Methodology

The forces and moments induced by a TLV flow acting on a rigid HAWT model were studied experimentally in The Wind Engineering, Energy and Environment (WindEEE) Dome at Western University in Canada (Hangan, 2014). A large-scale TLV, the so-called Mode B Tornado, was employed as the flow acting on the rigid wind turbine model under two rotor operational conditions and five radial distances. The experimental cases designed for this research were aimed to emulate the typical extreme conditions experienced by large commercial wind turbines installed in wind farms during severe atmospheric events. These experimental cases were also defined taking into consideration future DLC for TLV flows analogous to the DLC for ABL flows included in the IEC standard 61400-1, where the loads over a range of wind speeds, turbulence conditions and design situations are analyzed. For instance, DLC 1.1 and 1.2 embody the requirements for loads resulting from atmospheric turbulence that occurs during normal operation of a wind turbine throughout its lifetime (NTM). DLC 1.3 embodies the requirements for ultimate loading resulting from extreme turbulence conditions. In DLC 6.1-6.4 the rotor of a parked wind turbine is either in a standstill or idling condition and extreme win speed models shall be considered.

2.3.1 The WindEEE Dome

The WindEEE Dome is a novel three-dimensional testing wind facility capable of reproducing ABL flows and non-synoptic wind systems such as tornadoes and downbursts. It possesses an inner and an outer hexagonal chamber of 25 and 40 meters in diameter, respectively. The first chamber is employed as the test area, and the outer ring serves to supply and recirculate the flow for the main fans. One of the six walls of the facility is instrumented with 60 fans arranged in a matrix of 4 rows and 15 columns, the so-called 60-fan wall. Additionally, the chamber has 40 peripheral fans distributed at the lower part of the five remaining walls, which actions can be combined with that of six large fans placed around an upper chamber which communicates with the main chamber through a mobile bell-mouth opening.

By virtue of its unique hexagonal design, WindEEE Dome can operate in two different configurations: as ABL wind tunnel or in axis-symmetric mode. In the most conventional configuration, the 60 fans of 0.8 m in diameter installed in the 60-fan wall of 14 m by 4 m can reproduce ABL flows of scales from 1/2000 to 1/1 similar to a conventional wind tunnel. However, the WindEEE Dome's most valuable attribute is the ability to reproduce axis-symmetric non-conventional flows such as tornadoes and downbursts. In the axis-symmetric mode, the six fans located in the upper plenum can push or pull air into or out of the inner chamber to simulate vertical flows. When the WindEEE Dome pulls air out of the inner chamber combined with the action of directional louvres placed at the lower level of the main chamber it is capable of reproducing TLV flows of variable length scales, intensities, and geometric structures by using two tornado modes: Mode A and Mode B. In Mode A, the six fans located in the upper plenum create a suction pressure that provides an updraft in the inner chamber. Directional louvers installed on each of the peripheral fan nozzles redirect the flow creating a rotating motion component that shapes the tornado vortex. In relation to Mode B, the updraft suction created by the upper plenum fans is coupled with a flow injected by the peripheral fans, which push the air into the inner chamber at a controlled speed and direction. This additional airflow increases the angular momentum of the swirling flow field. Consequently, the aspect ratio (a), the length scale (λ_L), and the velocity scale (λ_U) could be modified (Ashrafi et al., 2021).

2.3.2 Large-scale Mode B Tornado

The Mode B Tornado used as the TLV flow in this research has been categorized as an EF2 tornado. Despite the existence of tornadoes with greater devastating power than EF2 tornadoes, it is unreasonable to over-design wind turbine structures for such rare wind events due to their low probability of occurrence. Therefore, the current study opted to work with the Mode B Tornado since tornadoes EF2 or less affect more frequently buildings, civil structures, and wind turbines.

The scale properties of the Mode B tornado were obtained by matching the radar data of the tornado event that occurred near Russell, Kansas (RK), on 25 May 2012 (Kosiba &

Wurman, 2013) and the velocities obtained in the WindEEE Dome testing chamber. The velocity scale was obtained by comparing the maximum velocity registered in the real tornado to the maximum velocity measured in the physical simulations. The proper geometric scale of the Mode B tornado was calculated by determining the intersection of the two length scale ratios in tornadoes: the ratio of the radii corresponding to the maximum velocity and the ratio of heights corresponding to the maximum velocity between the simulated and full-scale tornadoes. This matching procedure was established in the studies conducted by Hangan and Kim (2008) and expanded by Refan et al. (2014) for tornadoes of length scales between 1/150 to 1/300 and velocity scales of the order of approx. 1/3. The Mode B simulated tornado uses additional angular momentum introduced by the peripheral fans at WindEEE and is able to produce larger tornadoes, of length scales of the order of 1/50 to 1/70 and with lower velocity scales of the order of 1/6.5 (Ashrafi et al., 2021). The use of the large-scale Mode B tornado was motivated: (i) for testing larger structures including wind turbines up to 110 m in full scale rotor diameter as for the present study and (ii) for aeroelastic studies on structures for which the Froude number similarity needs to be fulfilled.

Using a length and velocity scale of $\lambda_L = 50$, and $\lambda_U = 6$ respectively, the laboratory test measurements registered a time-average value of the maximum tangential velocity ($U_{max,t}$) of 7.13 m/s with $S = 0.85$. This velocity was found at a height (z_{max}) of 0.1 meters above the floor of the testing chamber and a radial distance (r_{max}) (radius of the maximum tangential velocity) of 1.2 meters from the vortex center of the TLV flow (Ashrafi et al., 2021). However, the value of the maximum velocity was found to be relatively constant with height.

2.3.3 Wind turbine model

The rigid wind turbine model has been studied intensely before at Western University for its characterization, straight flow performance, and structural behaviour under both straight and extreme gust winds (Shirzadeh et al., 2020; Refan & Hangan, 2012). The term ‘rigid’ means that the wind turbine model used in the experimental tests is not a representative aeroelastic model. Therefore, the resonant component is not captured in

the tests. A study conducted by Xu and Ishihara (2014) have shown a minor contribution of the resonant component for wind turbines subjected to ABL. However, further studies are needed to assess the dynamic behaviour of an aeroelastic model of HAWT under tornadoes. The rigid wind turbine model is an upwind, three-bladed HAWT with a rotor of 2.2 m in diameter and a variable hub height (H_{hub}) set at 1.5 m. It can produce 900 W of rated power at 12.9 m/s and a peak power output of 1200 W at 17 m/s. The wind turbine was designed originally as a full-scale wind turbine for small applications. However, the wind turbine model represents a rotor diameter of 110 m when it is scaled up using the $\lambda_L = 50$, corresponding to comparable sizes of currently used large multi-MW wind turbines. At this scale, the HAWT wind turbine is similar to the HAWT used in the TUM numerical modelling (Campagnolo & Biegle, 2019). The wind turbine possesses an AC three-phase generator inside the nacelle and an external power terminal, which converts the current from AC to DC and can modify the voltage. Moreover, the Tip Speed Ratio (TSR) of the rotor can be specified by manipulating the terminal using power resistors to simulate a power load.

As the wind turbine was designed originally for small applications, it should be mentioned that the design of the airfoils and the blade aspect ratio are not identical to those found in the slender blades used in multi-MW wind turbines in the industry. A larger aspect ratio, which is typical in small wind turbines, can represent a slight disagreement in the overall load measurements. Additionally, it does not provide blade pitch control and yaw orientation, which limits the reproduction in the test cases of commonly used strategies of protection against severe atmospheric events.

2.3.4 Experimental setup

The rigid HAWT model was installed at the center of the WinDEEE Dome inner chamber. It was fixed to the ground, and the wind turbine rotor was oriented towards the positive direction of the Y-axis as shown in Figure 7.

In order to avoid disturbance in the flow caused by the wind turbine metallic legs, they were removed, and the wind turbine tower was connected to a base below the platform of the testing chamber. This means that the rigid wind turbine model must remain in the

same position. Therefore, to test the different radial distances (r) along the X-axis, the bell mouth located on the ceiling of the chamber was moved instead. To set the 5 radial distances, the bell mouth was displaced 0.4 meters in each case positioned it at 0.0 m, 0.4 m, 0.8 m, 1.2 m, and 1.6 m from the HAWT tower. Figure 7 and Figure 8 show the radial distances and the coordinate system employed to identify the loads acting on the rigid HAWT model and its dimensions.

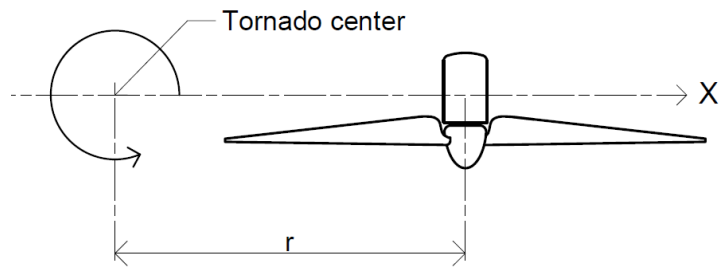


Figure 7 Experimental setup scheme

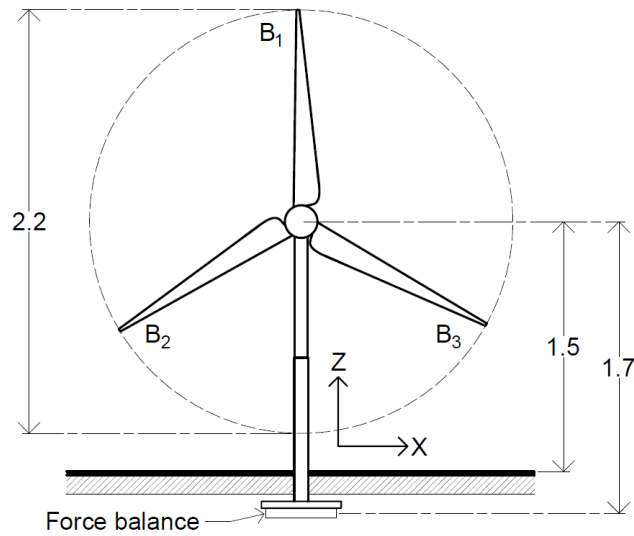


Figure 8 Small scale horizontal axis wind turbine

The radial distances were defined by considering the size of the wind turbine rotor of 2.2 in diameter. These positions allowed the $U_{max,t}$ of the TLV to impact the wind turbine from one edge to edge of the rotor swept area to study the hypothetical direction change

in the yawing moment. At each of the five radial distance positions, the overall loads acting on the rigid HAWT model were obtained under two rotor operational conditions: Parked and Idling condition. Table 2 describes the 10 test cases.

The IEC 61400-1 defines the parked condition as a standing still state for the wind turbine rotor. This condition was achieved by taping one blade to the nacelle. The azimuthal position or phase angle γ of the rotor blades, defined as the angle between the vertical Z-axis aligned with the wind turbine tower and the taped rotor blade, was set at $\gamma = 0^\circ$. According to Hu, Tian, and Ozbay (2019), the maximum induced loads (thrust and bending moment) by ABL flows acting on a parked HAWT were achieved at $\gamma = 0^\circ$. Therefore, the phase angle was set to 0° to accomplish the higher induced loads by the tangential component in the tornadic flow. Note that given the fact that the pitch angle cannot be varied for the test, the parked condition achieved is not identical to the standard park condition.

Table 2 Experimental test cases

Test case	Rotor condition	Radial distance (meters)
Test 1	Parked	0.0
Test 2	Parked	0.4
Test 3	Parked	0.8
Test 4	Parked	1.2
Test 5	Parked	1.6
Test 6	Idling	0.0
Test 7	Idling	0.4
Test 8	Idling	0.8
Test 9	Idling	1.2
Test 10	Idling	1.6

The Idling mode is defined when the wind turbine rotor is slowly rotating and disconnected from any electrical load, not producing power. However, the test wind turbine was protected by the use of resistors located in an external driver box set at 5 ohms ensuring the rotation at the low TSR=1.1. This condition does not differ

considerable from real idling scenarios when the rotational speed needs to be reduced or stopped by aerodynamics means.

In all cases, the instantaneous loads acting on the wind turbine were measured using a force-moment sensor model JR3 75E20s4-M125J-EF. The force sensor was installed at the base of the wind turbine model, and it captured the forces and moments induced by the stationary Mode B Tornado in the X-axis, Y-axis, and Z-axis directions using 6 analogue channels. The signals were gathered to one data logger at a 1250Hz frequency for 120 seconds for each run. Additionally, the rotor speed of the rigid HAWT model was obtained by using a light photoelectric proximity sensor (Autonics BR200-DDTN). This sensor, installed in the wind turbine tower, provides a pulse when it detects a light reflection from each blade passing in front of the HAWT tower. Figure 9 shows the rigid HAWT model orientation and position in the WinDEEE Dome, the 60-fans wall in the background, and the bell mouth at the top. Figure 10 shows the instrumentation installed with the rigid HAWT model.



Figure 9 Position of the wind turbine in the WinDEEE Dome test chamber

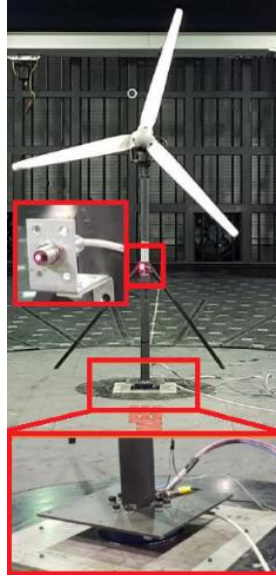


Figure 10 Force-balance and light sensor location in the wind turbine

2.3.5 Uncertainty analysis

The JR3 force-moment sensor installed at the base of the HAWT tower possesses a nominal accuracy of 0.25% based on the maximum rated load for each axis, which corresponds to 6,000 N and 1,100 Nm for the force and moment measurements, respectively. Therefore, a maximum error of 15 N and 2.75 Nm could represent a high possible uncertainty. However, a calibration process was performed by the JR3 company per request, by applying a 58.75 Nm moment repeatedly in the positive and negative direction of the X-axis. The calibration, trying to simulate close values to those obtained in this research, reported a ± 0.12 Nm error on average. This JR3 force-moment sensor was selected due to its size. The 19 cm in diameter of this sensor made possible the mounting of the rigid HAWT model directly on its surface, which could result very challenging for similar sensors designed for smaller rated loads. Only the X-axis bending moment will be presented in the results discussion as the other loads have small mean values that could lead to unacceptably uncertainties. However, normalized comparisons are presented.

2.4 Results and discussion

2.4.1 TLV-induced moment

The mean tower-base moment in the three axis directions acting on the rigid HAWT model at five radial distances with an idling rotor induced by the Mode B Tornado are presented in Figure 11. The mean bending moment (M_X) is the component that is the most important in terms of magnitude and features the major variation as the radial distance increases and the rigid HAWT model approaches to r_{max} . This moment is highly correlated to the U_t component of the Mode B Tornado, which is the flow component with the highest velocities in the TLV flow, as Figure 11 and Figure 12 show.

Figure 12 shows a velocity increment in the U_t component until the maximum radius position is reached at 1.2m, beyond that point and according to literature (Gillmeier et al., 2018) the tangential velocity should be continuously decreasing until it dissipates. Although the radius of maximum mean tangential velocity r_{max} is located at 1.2 m, the highest bending moment occurs at 1.6 m. This is the result of higher U_t speeds integrated in the swept area of the rotor at 1.6 m and vicinity due to smooth changes in the tangential velocities of the Mode B Tornado around 1.2 m and 1.8 m, see Figure 12.

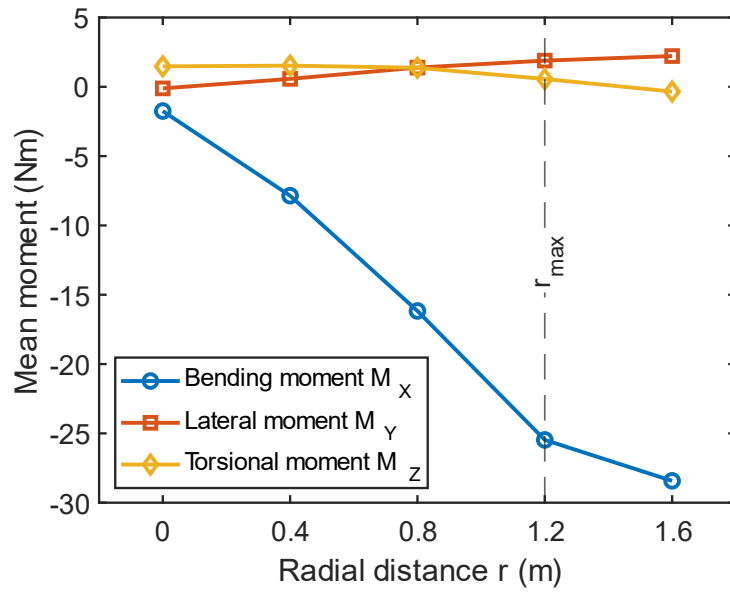


Figure 11 Mean moments at the tower base on the idling wind turbine at five radial distances from the tornado center

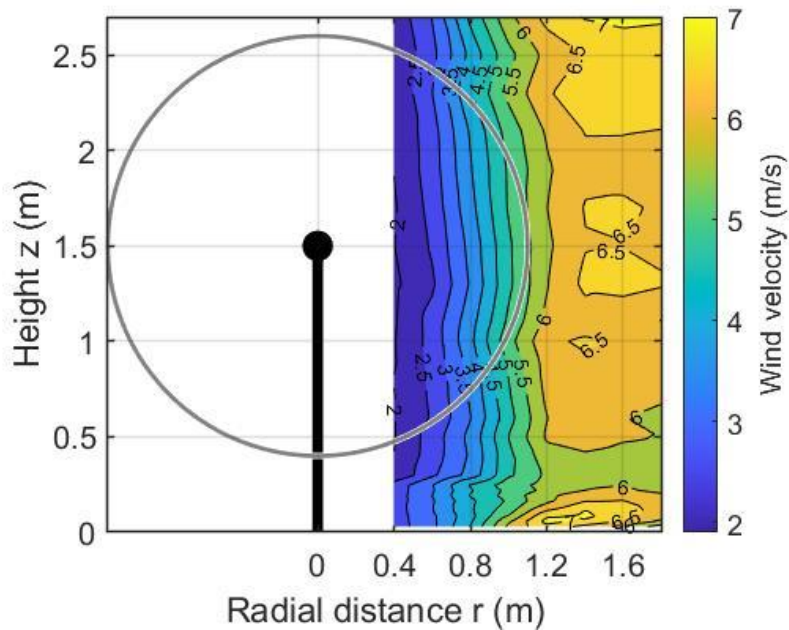


Figure 12 Tangential velocity contours of Mode B Tornado (m/s)

The additional angular momentum of the swirling flow field in Mode B Tornado produces smoother variations on S , almost constant around 1.5, and U_t around 7 m/s.

Similarly, the velocities of U_t on the swept area of the rotor dominate the tower-base torsional moment (M_z) as it is discussed further.

Figure 13 shows the tower-base bending moment at the five radial distances for the two rotor conditions, parked and idling, and the TSR of the wind turbine for the idling cases. The TSR is the ratio given by dividing the rotational speed ω of the wind turbine blades by the speed of the incoming wind at the hub height, U_{hub} expressed by:

$$\text{TSR} = \frac{\omega R}{U_{hub}} \quad (3)$$

where R is the rotor radius.

Note that when the rigid HAWT model was placed at the TLV center and at the radial distances of 0.4 m and 0.8 m, there was no rotational movement, hence the loads were nearly identical between both rotor conditions. However, passing the radial distance of 0.8 m, the idling rotational speed peaks up as the rigid HAWT model is affected by higher tangential velocities (see also Figure 12). This is similar to the results obtained by Hu, Tian, and Ozbay (2019) who found the difference between parked and idling cases being dependent on the TSR. The bending moment for the idling condition increases in comparison to the parked condition with increasing radial distance and TSR. Note that the TSR in the idling cases was limited by using a resistance of 5 ohms in order to avoid mechanical damage in the wind turbine structure due to high velocities generated by the TLV flow. While the present parked condition does not include a park pitch position, it is clear that the parked condition has the effect of reducing the overall base bending moment.

The power spectrum of the bending moment at a radial distance of 1.6 m for both idling and parked rotor allows assessing the influence of the TSR to the tower-base bending moment. The frequency distributions for the two rotor conditions are similar except for a clear peak located at a frequency of 3 Hz as depicted in Figure 14. This frequency corresponds to the wind turbine rotor frequency of the blade (f_b) passing in front of the wind turbine tower.

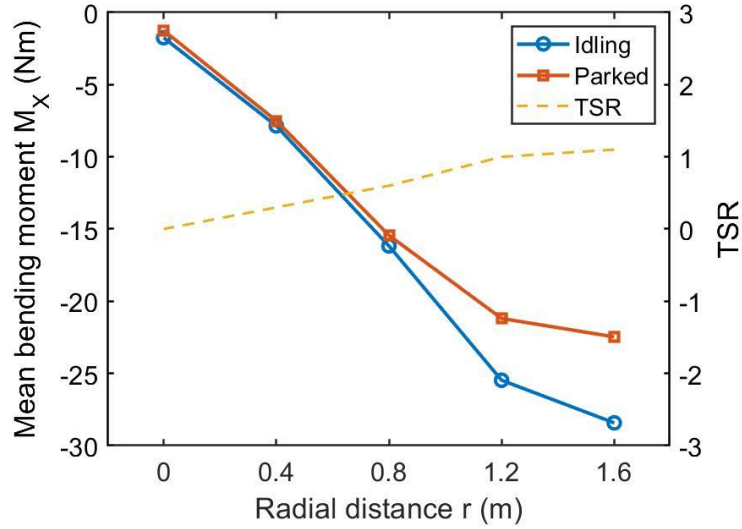


Figure 13 Mean bending moments and TSR for idling and parked conditions

The power spectrum of the bending moments also shows additional peaks at the medium frequencies that identifies the influence of the vortex shedding (f_w) and natural frequency of the cylindrical tower (f_n). The approximated vortex shedding frequency of 20 Hz is calculated based on the Strouhal number:

$$f_w = \frac{U_{hub} St}{l_T} \quad (4)$$

l_T being the projected tower diameter normal to the flow direction (0.075 m), assuming U_t as the dominant flow direction and a time-averaged U_{hub} of 6.5 m/s. The St value was set to 0.21 typical for circular cylinders in the range of Reynolds number (Re) of $5 \cdot 10^2 < Re < 5 \cdot 10^5$ (Roshko, 1953). The $Re = 3.3 \cdot 10^4$ value for these tests was obtained by:

$$Re = \frac{\rho U_{hub} l_T}{\mu} \quad (5)$$

where ρ and μ are the air density (1.225 kg/m^3) and dynamic viscosity ($1.81 \cdot 10^{-5} \text{ kg/ms}$), respectively.

The natural frequency was obtained by considering an undamped wind turbine tower as:

$$-M\omega^2 \cdot A \cos(\omega t) + K \cdot A \cos(\omega t) = f(t) \quad (6)$$

Substituting an external applied force $f(t) = 0$, in Eq. (6), then $A \cos(\omega t) = 0$. Placing ω on the left side

$$-M\omega^2 + K = 0 \quad (7)$$

$$\omega = \sqrt{\frac{K}{M}} \quad (8)$$

where M is the wind rotor mass (9 kg), and K for a uniform beam with one end free (cantilever) is:

$$K = \frac{3EI_{xx}}{l_T^3} \quad (9)$$

E stands for the modulus of elasticity ($205 \cdot 10^9 \text{ N/m}^2$) and I_{xx} the area moment of inertia for a hollowed steel tower of constant section ($1.5 \cdot 10^{-6} \text{ m}^4$). Therefore, the approximated 30 Hz frequency in Hertz is defined by:

$$f_n = \frac{1}{2\pi} \sqrt{\frac{3EI_{xx}}{l_T^3 M}} \quad (10)$$

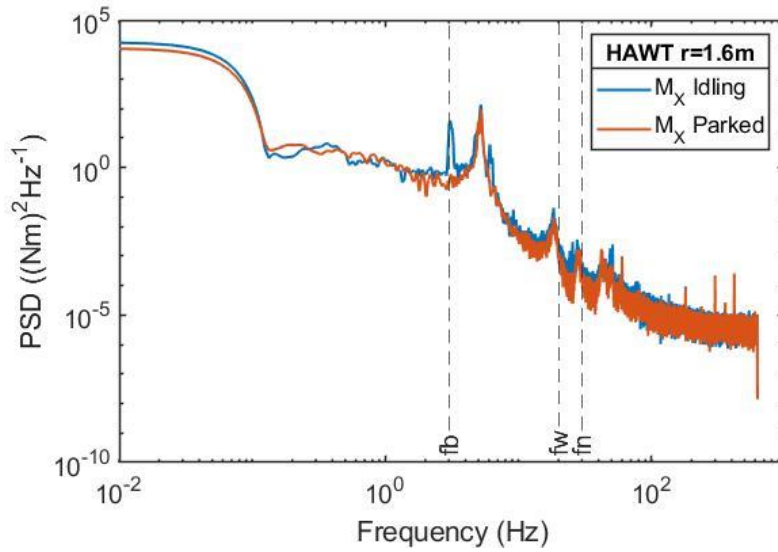


Figure 14 Power spectral density of the bending moments

2.4.2 Lateral and torsional moment dependency on the three-dimensional TLV flow

Figure 15 and Figure 16 show the normalized lateral and torsional moments exerted at the tower base in the Y-axis and around the Z-axis, respectively.

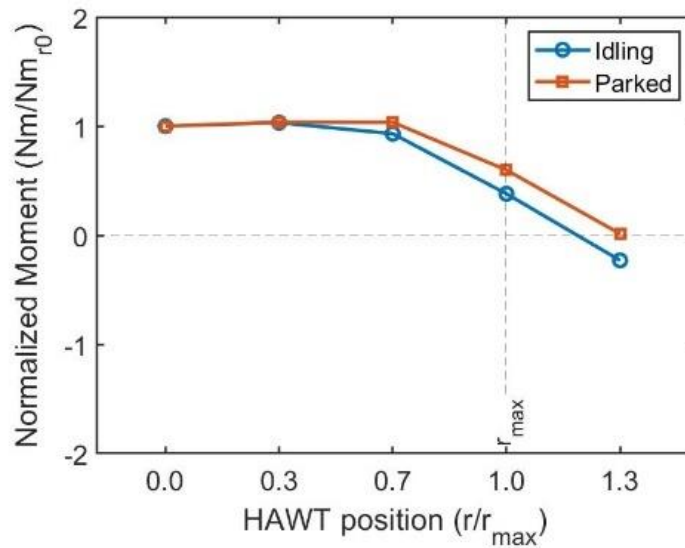


Figure 15 Normalized torsional moment

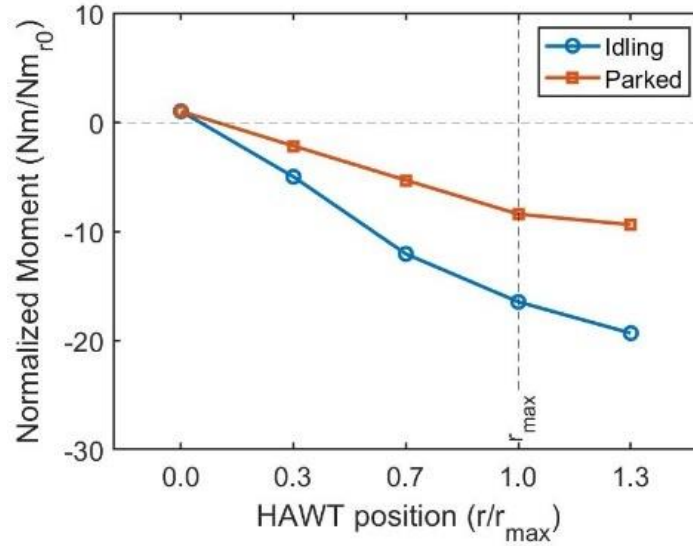


Figure 16 Normalized lateral moment

The moments were normalized by their corresponding values at $r = 0$ (rigid HAWT model placed at the TLV center). At this location, the torsional moment (M_Z) reached the maximum value due to the axis-symmetric swirling flow dominated by U_t (Figure 15). Additionally, the lateral moment (M_Y) is approximately zero due to the equilibrium condition reached by the lateral forces generated by the U_r component approaching from all direction towards the TLV core center. As expected, the torsional moment M_Z changes its sign as the relative position between the wind turbine and the center of the vortex changes from $r/r_{max} < 1$ to $r/r_{max} > 1$. The $U_{max,t}$ found at r_{max} changes its striking surface area from one side to the other side of the hub in the swept area. This creates a horizontal shear that changes the wind velocity gradient in the lateral position of the swept area shifting the torsional direction.

Figure 16 shows a continuous moment increase in the absolute values of M_Y as the radial distance approaches to r_{max} . However, Figure 17 shows that the vertical profiles of U_r and U_a do not establish a clear dependency with respect to r (Ashrafi et al., 2021). Therefore, the variations in M_Y are generated largely by U_t . Although U_r and U_a affect the rigid HAWT model, their velocities are considerably inferior to U_t . These moment variations follow similar trends as for the bending moment, M_X , with a continuous

increase up to r_{max} , and with a lesser increase out of the tornado core. Also, the lateral moment in the parked rotor case is lower compared to the idling case and that the difference between the two increases with radial distance.

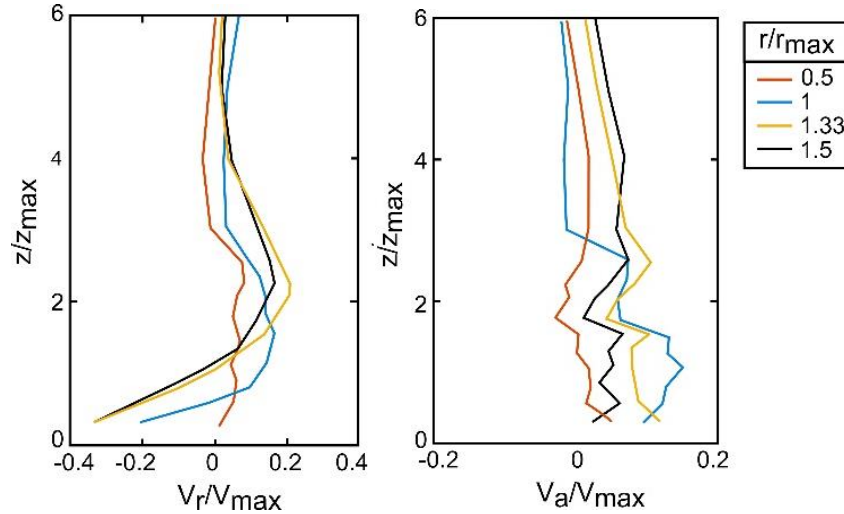


Figure 17 Radial (Left) and axial (Right) vertical velocity profiles for different radii

2.4.3 Preliminary comparison between uniform, ABL and tornado induced bending moments

The bending moment coefficients at the tower base for the rigid HAWT model at the highest loading positions at r_{max} and $r/r_{max} = 1.3$ were compared to an ABL and uniform flow with similar wind velocity, length scale, and rotor conditions in order to identify the effects on the wind turbine systems on different wind profiles.

The bending moments coefficients for a uniform vertical profile flow were obtained experimentally at the WindEEE Dome facility employing the same rigid HAWT model, and the idling rotor condition was set at the same TSR (1.1) at a constant incoming wind velocity of 5 m/s. The ABL case was obtained from an experimental test at the Iowa State University completed by Hu, Tian, and Ozbay (2014). The ABL flow corresponds to a reproduction of an ABL onshore flow defined by exponent of 0.16 for the Power Law corresponding to an open terrain. Due to the dependency of the wind speed on z , the wind speed was set at 4.5 m/s for the incoming wind speed at H_{hub} . Note that instead of using an idling rotor in the ABL test, a rotor in power production condition was used, set at an

optimum TSR=4.6 for that specific wind turbine. The corresponding coefficients for a TLV flow were obtained using the Mode B Tornado discussed previously, specifically for the cases at r_{max} and $r/r_{max} = 1.3$. Figure 18 shows the normalized wind vertical profiles for the three different wind flow cases.

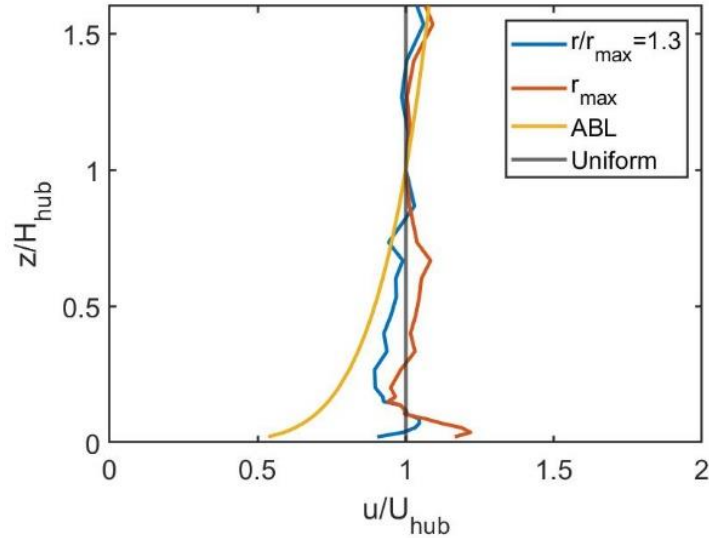


Figure 18 Normalized wind vertical velocity profiles

In order to compare the bending moments, the moment coefficients were calculated by using Equation 11, a conventional expression adopted for wind turbine load analysis (Hu et al., 2019).

$$C_M = \frac{M_x}{\frac{1}{2} \rho U_{hub}^2 \pi R^2 H_{hub}} \quad (11)$$

where M_x is the bending moment, R is the rotor radius, and the reference velocity, U_{hub} , was defined as the incoming wind speed at H_{hub} for each wind flow case.

The lowest mean C_M was found in the ABL flow case. It was clear that the energy distribution in the vertical wind speed gradient presented in the ABL profile produced lower loads than the other cases from H_{hub} to ground level. Although the wind speed in the ABL profile is higher in contrast to the TLV and the uniform flows at the upper part

of the wind turbine rotor, which represent more than 90% of the total loads in a wind turbine system (Hu, et al., 2014), the distributed load acting along the HAWT tower is considerably lower than the constant load in the uniform case. As the TLV cases were overall similar to the uniform profile, the C_M were similar to the uniform case for idling conditions.

For all cases, the idling values were higher compared to the parked values. The C_M difference between the idling and parked rotor condition, Figure 19, shows a higher contrast in the ABL case with respect to slightly closest values in the TLV and uniform cases. The bending moment on the parked wind turbine in the ABL case is approx. 40% of the operating rotor case, while for the TLV cases it is 80% of the idling rotor. As noted before, the rigid HAWT model used for those two cases did not allow a blade pitch control and the blades were permanently fixed in the optimum power output position.

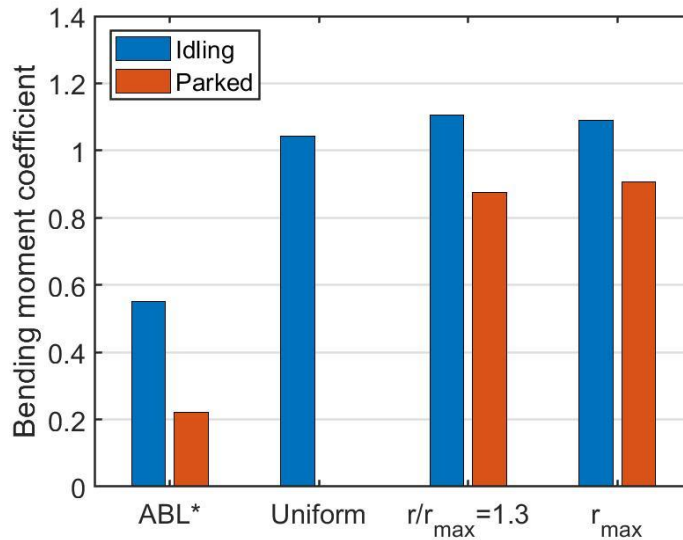


Figure 19 Bending moment coefficient comparison for an ABL, uniform, and tornado flow

2.4.4 Full-scale comparison of experimental and numerical induced maximum moments

The full-scale experimental moments were compared to those from several HAWT load scenarios designed by the TUM Wind Energy Institute, obtained by using numerical

methods. As mentioned in section 2.3, the research conducted by Campagnolo and Biegle (2019) calculated and ranked the absolute maximum values of the transient loads induced by the full-scale Mode B Tornado on blades, shaft, and tower on a HAWT with a 3.35 MW capacity, a rotor of 130 m in diameter, and a hub height of 110 m.

In order to compare the loads acting on the rigid HAWT model, the moments were scaled by:

$$M_p = M_m \cdot \lambda_U^2 \cdot \lambda_L^3 \quad (12)$$

where M_p is the full-scale prototype moment, M_m the moment acting on the model $\lambda_U = 6$, and $\lambda_L = 50$.

The test cases where the maximum bending moments were acting at the tower root are ranked in Figure 20. The highest moment found by the numerical methods (blue bar) occurred in a power production rotor at $r = 80$ m, when the TLV was approaching the wind turbine with a direction angle $\delta = 250^\circ$ at a translational velocity of 5 m/s.

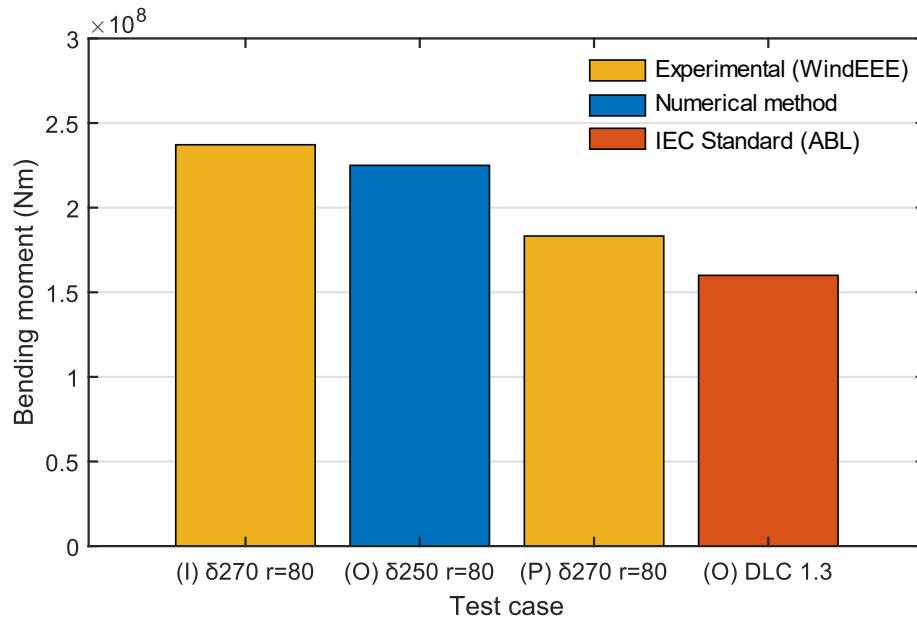


Figure 20 Experimental and numerical bending moment at the tower base. (I) Idling, (P) Parked, and (O) Operating

Similarly, the maximum moment on an idling and parked rotor obtained in this experimental study (yellow bars) were induced by a stationary tornado at $r = 80 \text{ m}$ and $\delta = 270$ position from the rotor plane. Therefore, in both numerical and experimental, the maximum bending moment was found at an identical radial distance slightly passing r_{max} and similar orientation with respect the rotor plane, due to smooth changes in U_t in Mode B Tornado from $r = 1.2 \text{ m}$ to $r = 1.8 \text{ m}$, as it was mentioned in section 2.4.1. Additionally, the maximum moment induced by DLCs included in the IEC standard 61400-1 for ABL flows was presented in the DLC 1.3 with a power production condition and the Extreme Turbulence Model (ETM). However, the bending moment induced by the DLC 1.3 was considerable inferior to that from Mode B Tornado. Note that the numerical tools used in the numerical analysis implemented a controller/supervisor system that reacted to temporal variations of inflow conditions by changing the generator torque, the blade pitch angle and nacelle orientation. Also, the rigid HAWT model used in the experimental tests in this research held a fixed blade pitch angle and yaw orientation. Consequently, the induced loads were higher than those from the numerical method and real conditions.

2.5 Conclusions

An experimental study was conducted to analyze the forces and moments induced by a TLV acting on a rigid HAWT model for idling and park conditions. Results showed that as TLV are three-dimensional flows with velocity speed gradients in the radial, vertical, and tangential direction, the moments at the base of the tower depend on the location and orientation of the wind turbine system with respect to the tornado vortex center. The mean bending moment (M_x), which was defined perpendicular to the wind turbine rotor plane, is the moment that is the most important in terms of magnitude and shows important variations as the radial distance increases and the rigid HAWT model approaches to r_{max} (1.2m). Hence, this moment is highly correlated to U_t tornado flow component. Secondly, it was indicated that the differences between the bending moment acting on an idling and a parked HAWT increase as the TSR for the idling case increases. Similarly, the lateral and torsional moments at the tower base depend on the U_t flow component radial distribution. In all cases the parked configuration produces lower

moments compared to the idling configuration. When comparing bending moment coefficients between ABL, uniform and TLV flow conditions it is found that the ABL produces the lowest C_M values while the uniform and TLV conditions produce similar values for the idling case. Also, the parked wind turbine in the ABL produces a 60% reduction in bending moment compared to idling conditions, while in TLV that reduction is only 20%. These results are limited by the TSR dependency which was limited to 1.1 for the uniform and TLV flow cases during the tests. Another limitation of the study relates to the fact that the pitch angle of the blades was the same for parked and idling conditions

Finally, this paper is part of a larger ongoing research program. The result will be used to validate a numerical model developed in house. The final objective is to develop load cases simulating the critical effects of tornadoes on wind turbines, which could be implemented in the design codes.

2.6 References

- AbuGazia, M., El Damatty, A., Dai, K., Lu, W., & Ibrahim, A. (2020). Numerical model for analysis of wind turbines under tornadoes. *Engineering structures*, 223, 111157. <https://doi.org/10.1016/j.engstruct.2020.111157>
- Ashrafi, A., Hangan H., Romanic, D., Kasab, A., & Ezami, N. (2021). Experimental investigation of large-scale tornado-like vortices. *Journal of Wind Engineering and Industrial Aerodynamics*, 208, 104449. <https://doi.org/10.1016/j.jweia.2020.104449>
- Bortolotti, P., Bottasso C.L. & Croce, A. (2016). Combined preliminary-detailed design of wind turbines. *Wind Energy Science*, 1(1), 71-88. <https://doi.org/10.5194/wes-1-71-2016>
- Campagnolo, F., & Biegle, H. (2019). Numerical study of the loads induced by tornadoes on a 3.5 MW wind turbine. *Research Report No. 1: Technische Universität München, Munich, Germany.*

- Chang, C.C. (1971). Tornado wind effects on buildings and structures with laboratory simulation. *Third International Conference on Wind Effects on Buildings and Structures*, 231-240.
- Church, C.R., Snow, J.T., Baker, G., & Agee, E.M. (1979). Characteristics of tornado like vortices as a function of swirl ratio: A laboratory investigation. *Journal of Atmospheric Science*, 36(9), 1755-1776.
[https://doi.org/10.1175/15200469\(1979\)036<1755:COTLVA>2.0.CO;2](https://doi.org/10.1175/15200469(1979)036<1755:COTLVA>2.0.CO;2)
- David-Jones, R.P. (1973). The dependence of core radius on swirl ratio in a tornado simulator. *Journal of Atmospheric Science*, 30(7), 1427-1430.
[https://doi.org/10.1175/1520-0469\(1973\)030<1427:TDOCRO>2.0.CO;2](https://doi.org/10.1175/1520-0469(1973)030<1427:TDOCRO>2.0.CO;2)
- Fujita, T. (1981). Tornadoes and downbursts in the context of generalized planetary scales. *Journal of the Atmospheric sciences*, 38(8), 1511-1534.
[https://doi.org/10.1175/1520-0469\(1981\)038<1511:TADITC>2.0.CO;2](https://doi.org/10.1175/1520-0469(1981)038<1511:TADITC>2.0.CO;2)
- Gillmeier, S., Sterling, M., Hemida H., & Baker, C. (2018). A reflection on analytical tornado-like vortex flow field models. *Journal of wind engineering and industrial aerodynamics*, 174 10-27. <https://doi.org/10.1016/j.jweia.2017.12.017>
- Haan, F.L., Balaramudu, V.K., & Sarkar, P.P. (2010). Tornado-induced wind loads on a low-rise building. *Journal of Structural Engineering*, 136(1).
[https://doi.org/10.1061/\(ASCE\)ST.1943-541X.0000093](https://doi.org/10.1061/(ASCE)ST.1943-541X.0000093)
- Hangan, H. (2014). The Wind Engineering Energy and Environment (WindEEE) Dome at Western University. *Wind Engineers JAWE*, 39(4), 350-351.
<https://doi.org/10.5359/jawe.39.350>
- Hangan, H., & Kim, J.D. (2008). Swirl ratio effects on tornado vortices in relation to the Fujita scale. *Wind and Structures* 11, 291–302
<https://doi.org/10.12989/was.2008.11.4.291>

- Hau, E. (2013). *Wind turbines: fundamentals, technologies, application, economics*. Springer.
- Hu, H., Tian, W., & Ozbay, A. (2014). An experimental investigation on dynamic wind loads acting on a wind turbine model in atmospheric boundary layer winds. *32nd ASME Wind Energy Symposium*, 1-8. <https://doi.org/10.2514/6.2014-1221>
- Hu, H., Tian, W., & Ozbay, A. (2019). A wind tunnel study of wind loads on a model wind turbine in atmospheric boundary layer winds. *Journal of Fluids and Structures*, 85, 17-26. <https://doi.org/10.1016/j.jfluidstructs.2018.12.003>
- International Electrotechnical Commission (IEC). (2007). *Wind turbines part 1: design requirements (IEC) 61400-1*.
- International Renewable Energy Agency (IRENA). (2019). *Renewable capacity statistics*.
- Jischke, M.C., & Light, B.D. (1983). Laboratory simulation of tornadic wind loads on a rectangular model structure. *Journal of Wind Engineering and Industrial Aerodynamics*, 13(1-3) 371-382. [https://doi.org/10.1016/0167-6105\(83\)90157-5](https://doi.org/10.1016/0167-6105(83)90157-5)
- Kosiba, K., & Wurman, J. (2013). The three-dimensional structure and evolution of a tornado boundary layer. *Weather and Forecasting*, 28(6) 1552-1561. <https://doi.org/10.1175/WAF-D-13-00070.1>
- Lewellen, W.S. (1962). A solution for three-dimensional vortex flows with strong circulation. *Journal of Fluid Mechanics*, 14(3) 420-423. <https://doi.org/10.1017/S0022112062001330>
- Mishra, A.R., James D.L., & Letchford, C.W. (2008). Physical simulation of a single-celled tornado-like vortex, Part B: Wind loading on a cubical model. *Journal of Wind Engineering and Industrial Aerodynamics*, 96, 1258-1273. <https://doi.org/10.1016/j.jweia.2008.02.027>

- Refan, M., & Hangan, H. (2012). Aerodynamic Performance of a Small Horizontal Axis Wind Turbine. *ASME. J. Sol. Energy Eng.* 134(2): 021013. <https://doi.org/10.1115/1.4005751>
- Refan, M., Hangan, H., & Wurman J. (2014). Reproducing tornadoes in laboratory using proper scaling. *Journal of Wind Engineering and Industrial Aerodynamics* 135, 136-148. <https://doi.org/10.1016/j.jweia.2014.10.008>
- Refan, M., Hangan, H., Wurman, J., & Kosiba, K. (2017). Doppler radar-derived wind field of several tornadoes with application to engineering simulations. *Engineering Structures*, 148, 509-521. <https://doi.org/10.1016/j.engstruct.2017.06.068>
- Refan, M., & Hangan, H. (2018). Near surface experimental exploration of tornado vortices. *Journal of Wind Engineering and Industrial Aerodynamics*, 175, 120-135. <https://doi.org/10.1016/j.jweia.2018.01.042>
- Roshko, A. (1953). On the development of turbulent wakes from cortex streets. *Report No. NACA-TN-2913*. California Inst. of Tech. United States.
- Sarkar, P., & Razavi, A. (2018). Tornado-induced wind loads on a low-rise building: Influence of swirl ratio, translation speed and building parameters. *Engineering Structures*, 167, 1-12. <https://doi.org/10.1016/j.engstruct.2018.03.020>
- Sarkar, P., Sengupta, A., Haan, F.L., & Balaramudu, V. (2008). Transient loads on buildings in microburst and tornado winds. *Journal of Wind Engineering and Industrial Aerodynamics*, 96, 2173-2187. <https://doi.org/10.1016/j.jweia.2008.02.050>
- Shirzadeh, K., Hangan, H. Crawford, C., & Tari, P.H. (2020). Investigating the loads and performance of a model horizontal axis wind turbine under IEC extreme operational conditions. *Wind Energy Science*, 6, 477-489. <https://doi.org/10.5194/wes-6-477-2021>

- Wind Science and Engineering Center (WSEC). (2004). *A Recommendation for an enhanced Fujita scale*. The National Weather Service.
- Wiser, R., & Bolinger, M. (2019). (2018). *Wind technologies market report*. U.S Wind Energy Technologies Office.
- Xu, N., & Ishihara, T. (2014). Analytical Formulae for Wind Turbine Tower Loading in the Parked Condition by Using Quasi-Steady Analysis. *Wind Engineering* 38(3). <https://doi.org/10.1260/0309-524X.38.3.291>

Chapter 3

3 Experimental validation of a numerical model for tornado-induced loads on a HAWT for a variety of pitch and yaw angles

An experimental validation of a built-in-house numerical code, HIW-TUR, developed by AbuGazia et al. (2020) was conducted by evaluating the tornado-induced bending moments on a small, 2-meters diameter, horizontal axis wind turbine (HAWT) for a variety of yaw and pitch angles by employing a large-scale tornado simulation reproduced in The Wind Engineering, Energy and Environment (WindEEE) Dome at Western University, Canada. The HIW-TUR code was capable to identify the tornado position relative to the wind turbine as well as the maximum overturning moment at the base tower within the experimental instrumentation nominal accuracy of 0.25%. The validated HIW-TUR demonstrated that the maximum mean moments were found for radial positions larger than the core radius of the tornado vortex due to the positively skewed distribution of the tangential (U_t) tornado velocity component and that the straining actions on the blades and wind turbine could be reduce up to 40% by turning the blades to orient them in a direction parallel to the oncoming U_t air flow to minimize the drag, i.e. feathered position. By varying both the yaw angle of the rotor plane parallel to the stream-wise U_t wind direction and the blade in a feathered position the moments could be further reduced up to 80%.

3.1 Introduction

Wind power is one of the fastest-growing renewable energy sources. Its capacity installed globally has increased by a factor close to 75 in the last 20 years, and its annual expansion nearly doubled in 2020 compared to 2019 (IRENA, 2021). Utility-scale wind turbines typically installed in large wind farms are located in terrains free of high obstacles to benefit from steady and faster winds. However, opened landscapes are normally related to localized high-intensity wind (HIW) events such as tornadoes. Field observations have registered wind turbine failures during tornado events, for instance, the

May 14, 2012, Harper County, Kansas, tornado in the United States (NOAA, 2012). In addition, the continuous increase in the size of wind turbine rotors, results in an increase of simultaneous loads and dangerous cumulative effects produced by the inertial, aerodynamic, and gravitational forces on the wind turbine elements. These effects lead to higher risks of structural failure when they are exposed to localized HIW events, specifically tornadoes, due to the significant differences between the forces and pressures induced by three-dimensional flows in contrast to conventional synoptic winds.

Several experimental studies related to tornadoes-induced loads acting on a variety of structures have demonstrated that suction and dynamic pressures can be presented simultaneously on the various individual surfaces (Chang, 1971). The contrasting dynamic pressures are due to the additional swirl in the three-dimensional flow, causing peak loads higher than those by synoptic winds with same wind speed (Jischke, & Light, 1983). The peak loads on small buildings can be 1.5 times higher, and highly dependent on the position of the structure with respect to the tornado core center (Sarkar et al., 2008; Sarkar, & Razavi, 2018). The unique tornado wind characteristics involves several challenges for the structural analysis of their effects on wind turbine straining actions. The studies related to wind loads acting on wind turbines are, in general, based on synoptic winds and already incorporated in standards and design recommendations. However, tornadoes possess a three-dimensional flow with velocity gradients in the radial (U_r), vertical (U_a), and tangential (U_t), directions that vary in time and spatially. Consequently, each wind turbine element will experience different wind actions during a tornado event depending on their position and orientation with respect to the tornado core center. For instance, the maximum mean forces acting on each of the wind turbine blades, the wind turbine tower, or the overall overturning moment at the base of the tower can be generated by different tornado positions due to the different gradient distributions and peak locations of the U_r , U_a , and U_t , tornado velocity components. Furthermore, the direction and velocity of synoptic winds can be determined, so wind turbine rotors and blades can be oriented to reduce the aerodynamic loads produced by the wind. By contrast, tornadoes are random phenomena with unpredictable paths that make highly challenging the active control of the rotor plane orientation and blades with respect to the

oncoming wind. Regarding these spatial and aerodynamic dependencies, AbuGazia et al. (2020) identified the location of the maximum mean forces exerted by a stationary tornado acting from several positions around a wind turbine by using a built-in-house numerical model. It was found that the minimum mean forces acting on the blades occurred when the pitch angles were set at 15 degrees, and those forces were higher than those produced by the extreme wind load scenarios included in the IEC 61400-1 standard. More recently, Lopez et al. (2021) performed an experimental study to analyze the response of a small HAWT under a tornado wind field. A large-scale tornado simulation developed in WindEEE dome at Western University in Canada (Hangan, 2014) was employed to act on a small-scale wind turbine under two rotor operational conditions, idling and parked, at five radial distances from the tornado core center. It was observed that the overall forces and moments were dependent on the location and orientation of the wind turbine with respect to the tornado core center. The bending moment at the tower base was the most important in terms of magnitude and variation relative to the position of the HAWT and increased with the rotor Tip Speed Ratio (TSR). In order to extend a tornado-wind turbine analysis, an experimental validation of a numerical code is needed to produce more quantifiable statements with a satisfying level of agreement between computational results and experimental data. The present study therefore aims to experimentally validate the numerical model used in AbuGazia et al. (2020) by comparing the results with the information acquired in Lopez et al. (2021). The validation will allow the numerical model to predict the response of the tower and blades of HAWT for a variety of case studies. This general objective is subdivided in the following specific objectives:

- Validate experimentally the developed numerical model comparing the tornado-induced bending moment on a wind turbine under various locations.
- Analyze a HAWT using the developed numerical model to identify the tornado location that leads to the peak straining actions on the tower and blades for a variety of yaw and pitch angles.

- Determine the optimum pitch angle that leads to minimum straining actions on both the blades and the tower given the uncertainty associated with the tornado location.

This chapter is divided into five sections. Section 3.2 describes the characteristics and findings regarding the experimental analysis of the tornado-induced loads on a HAWT, which are employed for validation purposes. Section 3.3 provides the mathematical details of the numerical model and the validation discussion. In Section 3.4 a case study is explored in order to determine the optimum aerodynamic orientation of the wind turbine elements with respect to the tornado position to minimize the straining actions on blades and tower. Finally, the main conclusions are outlined in Section 3.5

3.2 Experimental tornado-induced loads on a HAWT

The forces and moments induced by a stationary tornado acting on the small-scale HAWT were captured in the X-axis, Y-axis, and Z-axis, under two rotor operational conditions and five radial distances (r) between the tornado core center and the wind turbine tower at 0.0, 0.4, 0.8, 1.2, and 1.6 meters. The two operational conditions are: Idling is defined by the IEC 61400-1 as a wind turbine rotating slowly and not producing power; and Parked as the condition of a wind turbine that is stopped, generally achieved by mechanical brakes and aerodynamic means by feathering the wind turbine blades. In spite of the pitch control absence in the small-scale HAWT used in the investigation, a brake mechanism was used to fulfil the parked condition. Figure 21 shows the experimental scheme with the independent variable r and the geometrical characteristics of the small-scale HAWT. The phase angle of the rotor blades, γ , defined as the counterclockwise angle between the Z-axis and the blade B_1 , was set at $\gamma = 0^\circ$. The experimental setup is described in detail in Chapter 2.

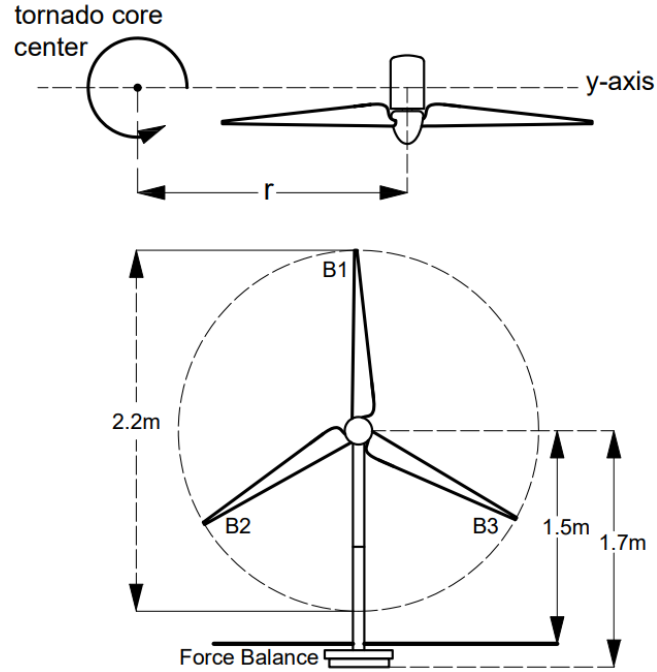


Figure 21 Scheme with the dimensions of the small-scale HAWT and the radial distance variable with respect to the tornado core center

3.2.1 Large-scale tornado characteristics

The tornado wind field used in the experimental test by Lopez et al. (2021) and in the numerical validation further detailed in Section 3.3 was performed by Ashrafi et al. (2021). It was based in the Russel, Kansas tornado event (RK) occurred on May 25, 2012 (Kosiba, & Wurman, 2013). Lee et al. (1999) characterized the RK event by using a ground-based velocity track display (GBVTD) analysis as an EF2 tornado with a maximum tangential velocity ($U_{max,t}$) of 46 m/s located at a radial distance (r_{max}) of 60 m and at a height distance from the ground (z_{max}) of 5 m.

In order to reproduce accurately the tornado wind field characteristics in laboratory scales, the geometric length scale λ_L was obtained by a matching process of two length scale ratios between full-scale data or prototype (subscript “p”) and a model reproduction (subscript “m”). The process proposed by Refan et al. (2014) considers the ratio of the core radius length where the maximum tangential is located (r_{max}): $f = r_{max,po}/r_{max,mo}$. The second length ratio is defined by the height corresponding the maximum tangential

velocity: $g = z_{max,p}/z_{max,m}$. Therefore, λ_L was determined based on the intersection of the two scales i.e., $f = g$. The scaling procedure applied to the RK tornado indicated that the tornado reproduced in WindEEE, the so-called Mode B Tornado, found a matching length scale (λ_L) at 1:50. The velocity scale (λ_U) of 1:6 was defined by the ratio between the maximum tangential velocity of the RK event and that of the Mode B tornado: $U_{max,t,p}/U_{max,t,m}$. As a result, the $U_{max,t} = 7.13$ m/s, was localized at $r_{max} = 1.2$ m and $z_{max} = 0.1$ m (Ashrafi et al., 2021). Figure 22 depicts the velocity contours of the radial (U_r), vertical (U_a), and tangential (U_t) Mode B Tornado. Finally, the time scale (λ_T) was defined by $\lambda_T = \lambda_L/\lambda_U$.

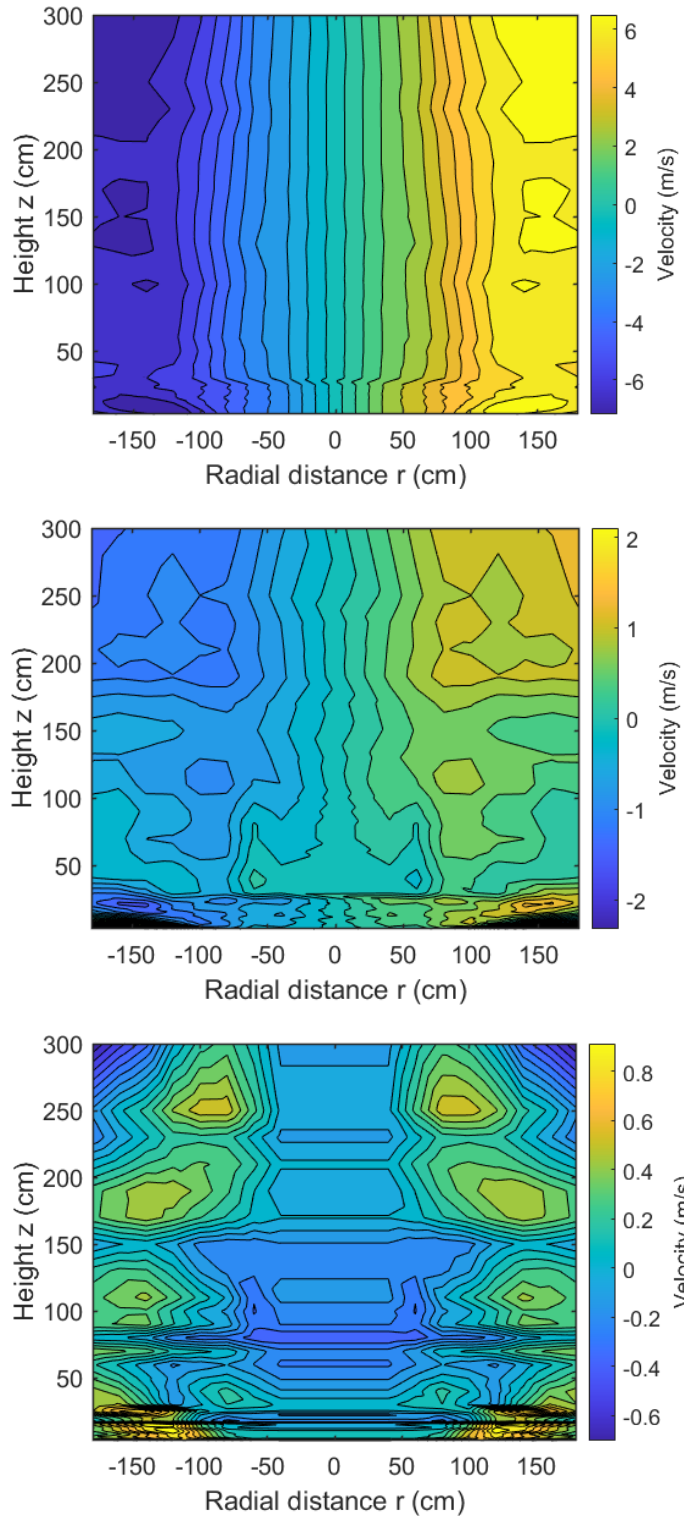


Figure 22 velocity component contours of Mode B Tornado: U_t (top), U_r (middle), U_a (bottom).

3.2.2 Wind turbine details

The wind turbine employed in the experimental test and modeled in the numerical analysis was a three-bladed HAWT of 2.2 m in rotor diameter and a hub height (H_{hub}) of 1.5 m supported by a hollowed cylindrical steel tower. It has been studied intensely before at Western University for its characterization, straight flow performance, and structural behavior under both straight winds and gusts (Refan, & Hangan, 2012; Shirzadeh et al., 2020). The blade length (l) is 1 m with a variable chord length, c , from root to tip of 12.7 cm and 5.4 cm, respectively. The rotor possesses twisted blades to compensate the absence of pitch and yaw active control. Refan (2009) reported the chord and twist angle distribution along the blade span as well as the airfoil profile of each section as Figure 23 shows the tip region of the blade ($0.58 < l < 1.03$) uses a FX-63137 profile, whereas the root region ($0.12 < l < 0.57$) uses a NACA-6515 for structural support. The blade twist angle varies from 34 to -3 degrees, from root to tip (Figure 23). For the current study, the wind turbine was assumed as a large Utility-scale wind turbine of 110 m in diameter and H_{hub} of 75 m by applying the $\lambda_L = 1:50$ used by the Mode B Tornado.

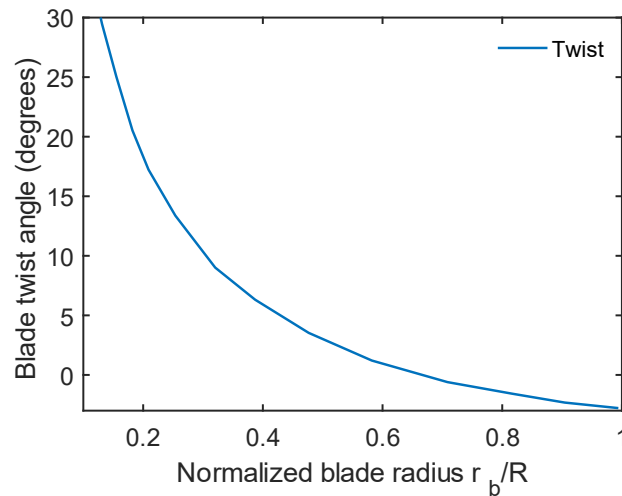


Figure 23 Twist angle and chord length distribution along the blade

3.2.3 Experimental tornado-induced loads on a HAWT

Although, a tornado is a three-dimensional wind field composed by U_r , U_a , and U_t , components, the overall straining actions on the wind turbine were highly correlated to the dominant U_t component, and therefore, to the relative position to the core center of the tornado. The time-average bending moment (M_x), which is due to the reaction perpendicularly to rotor plane of the wind turbine, is the most important in terms of magnitude and features the greater variation as r increases and the small-scale HAWT approaches to r_{max} . This correlation is attributable to the velocity distribution in the U_t component, as U_r and U_a are relative constant along the radial direction, with maximum velocity gradients of 0.6 m and 0.2 m, respectively. Additionally, r_{max} is located at $r = 1.2$ m, but the mean peak M_x , occurs at $r = 1.6$ m ($r/r_{max} = 1.3$). This is the result of the impinging of higher U_t speeds in the integrated swept area by the rotor at 1.6 m and vicinity due to a smoother and higher U_t velocity distribution in $1.2\text{ m} < r < 1.8\text{ m}$ as it is depicted in the velocity contours in Figure 22. Additionally, the bending moment for the idling condition increases with increasing r and the tip-speed ratio TSR. This difference is due to the related increment in the resulting wind speed impinging on the blades during operation.

3.3 Experimental HIW-TUR validation

The numerical code examined in the current research was originally developed to assess the behavior of transmission lines under tornado wind loading (Hamada et al. 2010), and it has been applied in several investigations at Western University (Hamada et al., 2011; Hamada et al., 2015; and Ibrahim et al., 2017). As an extension of this code, AbuGazia (2021) and Mostafa (2021) coupled the original nonlinear finite element code with the proper aerodynamic forces generated by the components of a typical HAWT, resulting in the HIW-TUR code, acronyms that stand for High-Intensity Wind (HIW) and Turbine (TUR).

In order to validate the application of the HIW-TUR code, the numerical base-tower M_x were compared with those from the experimental test obtained in the WindEEE Dome. The HIW-TUR code compares the M_x assuming a parked rotor condition at five radial

positions using the tornado flow field data obtained from the cobra probes measurements captured by Ashrafi et al. (2021) as the wind field input. There is no active pitch angle control in the small-scale HAWT, therefore the experimental validation was restricted to the predetermined blade position fixed at a 0-pitch angle. As a result, while the rotor was not moving this is not a proper “parked” condition for the HAWT and it is used as a case that can be validated between the numerical code and the experiments. As demonstrated in Section 3.2.3, M_x was the most important moment in terms of magnitude and variation in relation to the position of the HAWT with respect to the core center of the tornado. Consequently, M_y and M_z were not included in the validation analysis as they portrayed small moments near to 10% of M_x and small moments variations lower than 3 Nm along r .

The HAWT geometric and structural characteristics described in Section 3.2.2 were modeled in the HIW-TUR code as a circular hollow steel tower divided in two segments of constant diameter and thickness. The first segment at the base has an interior and exterior diameter of 6.5 and 7.0 cm, respectively. Meanwhile, the correspondent values for the top segment are 5.0 and 6.5 cm. Both sections with a 0.5 cm thickness. Additionally, the distance of 15 cm between the rotor disk plane and the wind turbine tower presented in the small-scale HAWT was included in the numerical analysis. The blades are embedded into the hub at a fixed pitch, and each of the blades was divided into 16 segments with variable c and equal spanwise length. The HAWT numerical model was positioned in a coordinate system built based on consideration of the for-aft direction as the X-direction and of the side-to-side direction as the Y-direction. This implies that the rotor plane was normal to the U_t component of the tornado wind field, as in the experimental test.

3.3.1 Description of the numerical code

The HIW-TUR code incorporates two modules designed to operate with tornadoes and downbursts as non-synoptic high intensity wind fields. The numerical code calculates the wind loads acting on the wind turbine blades by subdividing them into a discrete number of segments along the spanwise direction and considering each division as an

independent two-dimensional airfoil section. The wind-induced loads on each section are estimated by determining the aerodynamic lift (F_L) and drag (F_D) forces based on the two-dimensional airfoil theory. F_L and F_D on a random blade airfoil section (i) are calculated by:

$$F_{Lij} = \frac{1}{2} (C_L)_{ij} \rho c_i V_{ij}^2 l_i \quad (13)$$

$$F_{Dij} = \frac{1}{2} (C_D)_{ij} \rho c_i V_{ij}^2 l_i \quad (14)$$

where ρ is the air density, which is equal to 1.225 kg/m³; c is the chord length of the blade airfoil section (i); l is the length of the blade section (i); and V is the wind velocity acting on the element, with (i) and (j) representing the section number and the wind direction, respectively. C_L and C_D are the lift and drag coefficients, which vary depending on the geometry of the airfoil section (i) and the wind direction (j). Consequently, C_L and C_D are dependent on the angle of attack (α), which is defined as the angle between the airfoil chord and the wind direction. Figure 24 represents the force diagram of an airfoil section (i) and the pitch angle relation with the attack angle, which is calculated from:

$$\alpha_j = \varphi_j - \beta \quad (15)$$

where φ is the angle formed between the rotor plane and the wind direction, and β is the pitch angle of the blades.

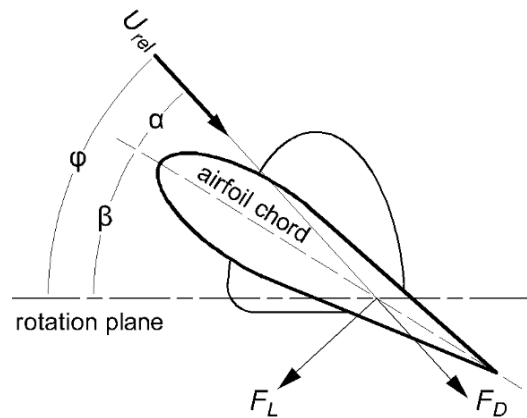


Figure 24 Force diagram of an airfoil section (i)

Utility-scale wind turbines can regulate F_L and F_D by changing the α angle in order to preserve the rated power output and for structural safety when the direction and velocity of the wind change. However, the cut-in speed and rated wind speed are of significance importance for wind turbines with fixed pitch angle and no active controls, where the optimum shape of wind turbine blades consists of airfoil sections of increasing thickness and twist angle towards the hub. Therefore, the HIW-TUR code incorporates the twist angle deflection as a geometrical characteristic of each airfoil section (i) to calculate the local angle of attack and F_L and F_D . Figure 25 shows the variable twist angle with respect to the position of the section relative to the total blade length L .

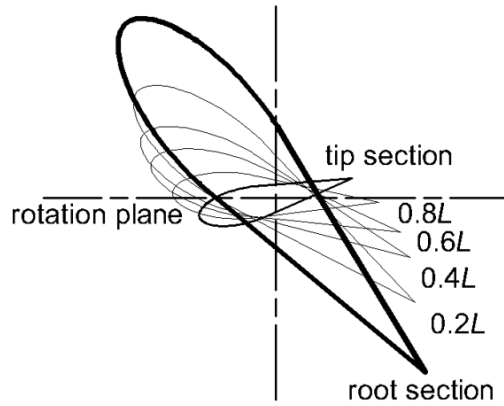


Figure 25 Variable twist angle with respect to the blade length L

The flow components V_{TN} , V_{RD} and V_{AX} from a tornado flow field are based on polar coordinates (R and θ). Those are resolved using equations 16-18 to obtain the velocity components (V_{ix} , V_{iy} and V_{iz}) acting on a specific airfoil section (i) in the code global coordinate system.

$$V_{ix} = (V_{TN})_i(\cos\theta) + (V_{RD})_i(\sin\theta) \quad (16)$$

$$V_{iy} = (V_{TN})_i(\sin\theta) - (V_{RD})_i(\cos\theta) \quad (17)$$

$$V_{iz} = (V_{AX})_i \quad (18)$$

For an airfoil section (i), the F_L and F_D forces are calculated by using equations 13 and 14, respectively, for each velocity component V_{ix} , V_{iy} and V_{iz} established by equations 16, 17 and 18. The Cartesian components of the F_L and F_D forces are dependent on γ for each blade, which are labeled correspondingly to the experimental small-scale HAWT showed in Figure 21. Additionally, the induced wind loads acting on the HAWT tower are estimated by the drag coefficient C_D for a smooth circular cylinder as a function of the Reynolds number as:

$$F_{ij} = \frac{1}{2} (C_D) \rho V_{ij}^2 A \quad (19)$$

where A is the projected area of the tower and C_D is approximated to 1.2 for an infinite circular cylinder in a $10^2 < Re < 10^5$ regime, which relates to $Re \approx 3 \times 10^4$ for the small-scale wind turbine tower as:

$$Re = \frac{\rho U_{t,tower} D_{tower}}{\mu} \quad (20)$$

where D_{tower} is the tower diameter, 0.07 m; $U_{t,tower}$ is the mean tangential velocity along the tower, 6.4 m/s; and μ is the dynamic viscosity, 1.81×10^{-5} kg/(m/s).

In summary, the forces on blades are resolved in a local coordinate plane and determined the flap-wise and edgewise moments at their roots. Similarly, the overturning and torsional moments at the tower base. First, the geometry characteristics of the wind turbine tower and blades are introduced into the HIW-TUR code, including the C_L and C_D data as a function of α . Secondly, the tornado flow field is added, and the flow components V_{TN} , V_{RD} and V_{AX} are generated for a specific R and θ . Subsequently, the velocity of the flow components acting on the airfoil sections and tower are obtained with respect to the Cartesian global axes x , y , and z in order to calculate the forces. Finally, the tower base and the blade root moments are evaluated. The detailed sequence of analysis and methodology used to calculate the forces and moments acting on the tower and blades can be consulted in AbuGazia et al. (2020).

3.3.2 Validation discussion

As discussed in Chapter 2, the force sensor JR3 75E20s4-M125J-EF possesses a nominal accuracy of 0.25% based on the maximum rated load for each axis, 6,000 N and 1,100 Nm for force and moment measurements, respectively. Therefore, it represents a maximum deviation of ± 2.75 Nm. Figure 26 shows the experimental and numerical bending moment at the tower-base of the small-scale HAWT at five normalized distances, including r_{max} for a “parked” condition. Results show an acceptable agreement between measured and simulated values inside the nominal accuracy of the experimental instrumentation, where the maximum absolute error of 2.24 Nm is presented at r_{max} . Accordantly with the experimental measurements, the HIW-TUR computed the maximum straining actions at $r/r_{max} = 1.33$.

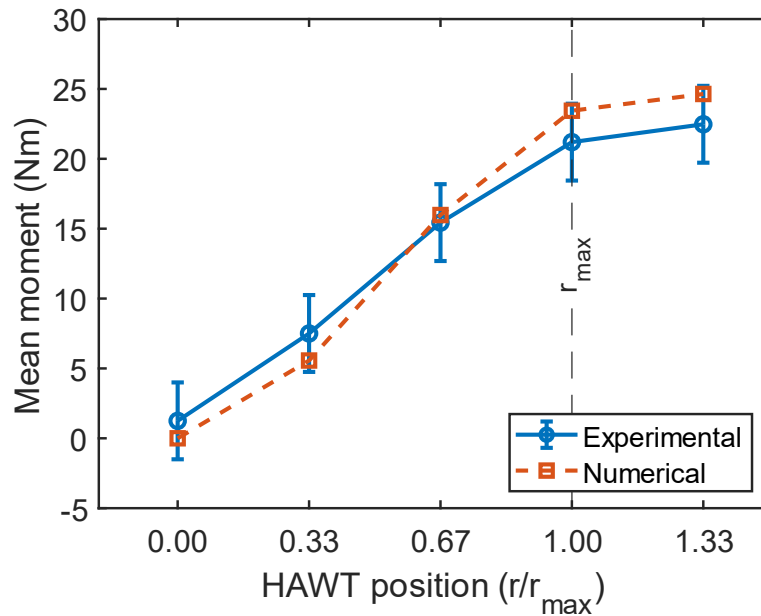


Figure 26 Experimental and numerical bending moment at the tower-base of the small-scale HAWT at five normalized distances

Meanwhile HIW-TUR underpredicted the response of the wind turbine system for low-speed and unsteady winds in close proximity to the tornado core center, the straining actions were overestimated for higher and steady flows, mainly U_t . Additional effects attributed to three-dimensional flows, especially for HAWT with small aspect ratio,

which are more susceptible to span-wise flow effects than utility-scale wind turbines with slender blades are neglected by the HIW-TUR code. Overall, the HIW-TUR code is capable of identify the tornado location that leads to the maximum straining actions on a HAWT within an acceptable range of accuracy, especially at a preliminary design stage. Additionally, it is assumed that the code can determine the optimum pitch angle that leads to minimum straining actions on both the blades and the tower with respect to a specific tornado location. Therefore, a case study was performed in order to overcome the experimental limitations for different scenarios varying the pitch angle, tornado approaching angle, yaw angle, and twist angle.

3.4 Case study

A case study was performed in order to identify the tornado location that leads to the maximum straining actions on the tower and blades of a HAWT for a variety of pitch and yaw angles. Consequently, this study will determine the optimum orientation of the blades of the wind turbine that leads to minimum straining actions on both the blades and the tower. The numerical model HIW-TUR was used to conduct the parametric analysis consisting of 172 cases. Following the sequence described in Section 3.3.1 the HIW-TUR model was used to obtain the forces acting on the blades and tower of a HAWT by manipulating three independent variables. The variables illustrated in the study scheme in Figure 27 are defined as following: δ , angle formed by the X-axis and the approaching angle of the tornado core center from 0° to 90° every 15° ; r/r_{max} from 0 to 3.5, every 0.5; and β from 0° to 90° every 15° .

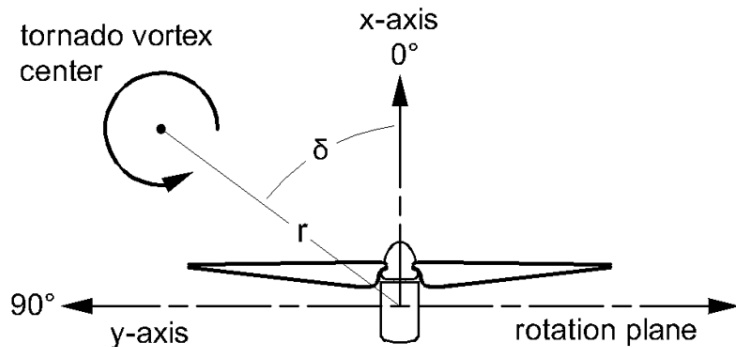


Figure 27 Scheme of the HAWT orientation with the variables r and δ

As the wind field data obtained from the experimental test consisted only in a two-dimensional plane along the X-axis, a computational fluid dynamic (CFD) simulation of a tornado wind field equivalent to the Mode B Tornado was reproduced in order to obtain the U_r , U_a , and U_t , components around the wind turbine elements in several spatial positions. In this study, a CFD simulation solving three-dimensional RANS equations using the RSM turbulence model was performed to reproduce the laboratory-scale Mode B tornado (Ezami et al., 2022). Figure 28 and Figure 29 show the vertical velocity profiles of the three velocity components of the CFD simulated tornado and a comparison between the U_t vertical profiles at r_{max} , respectively.

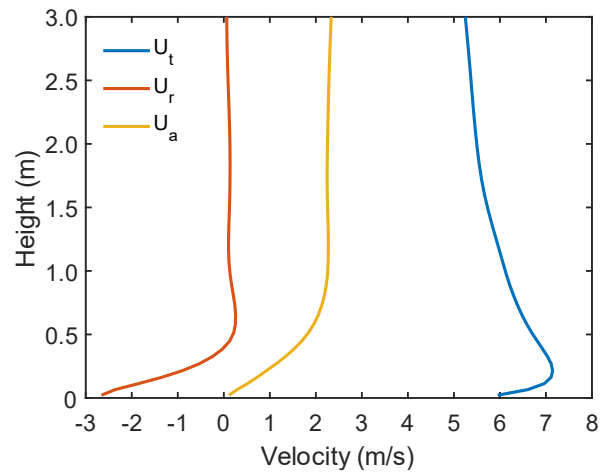


Figure 28 Vertical profiles of U_t , U_r , and U_a of the CFD simulated tornado

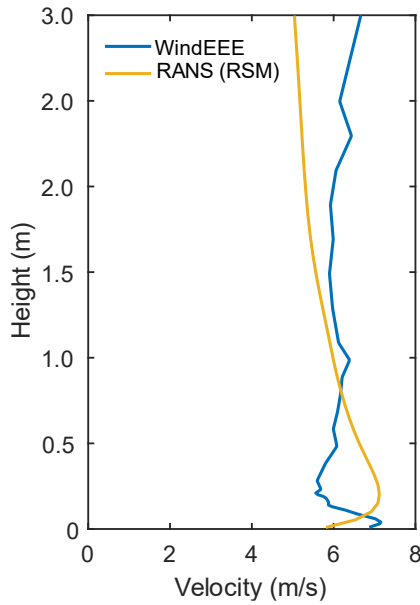


Figure 29 U_t vertical profiles of the Mode B tornado and CFD simulation at r_{max}

3.4.1 Case study discussion

The overall moment on the small-scale HAWT increases in a positively skewed bell shape distribution with maximum moments found at r/r_{max} positions between 1.2 and 1.8 (Figure 30). Since the wind field was based on the Mode B tornado, the maximum mean moment was likewise found $r/r_{max} = 1.5$ as result of the different slope of the horizontal U_t component profile and higher velocities impinging the wind turbine at the hub height in $1.2 \text{ m} < r < 1.8 \text{ m}$ as the U_t velocity contours show in Figure 22. Additionally, the overall moment is inversely proportional to the approaching angle of the tornado. As δ reaches 90° , the rotor plane is oriented perpendicularly to U_t increasing the drag force of the blade. However, note that the small-scale HAWT studied in the present research possesses fixed blades with a span-wise variable twist angle. Consequently, the perpendicular orientation of the wind turbine rotor with respect to the U_t tornado velocity component does not imply that the wind turbine blades are similarly in a perpendicular orientation to the U_t velocity component. Indeed, due to the twist angle presented in the blades, F_L and F_D vary along the span-wise direction. Furthermore, at certain span-wise location, the U_t component direction and the twist angle of the blade are aligned to produce the minimum drag force. The maximum moments are produced in

a wind turbine rotor orientation of $45^\circ < \delta < 75^\circ$ with a maximum at $\delta = 60^\circ$. Although a twisted blade produces a variable force along the span-wise direction, the total force produced by the whole blade can be matched to the force produced by a blade with constant pitch angle β . Figure 31 compares the bending moment at the tower base for a HAWT with span-wise constant β and identical airfoil characteristics against the current small-scale HAWT with twisted blades. It shows that the moment increases from feathered to perpendicular position of the blade with respect to U_t and the moment generated by the twisted blade is similar to that produced by a constant $\beta = 30^\circ$ position. This explains why the maximum moment was found at a wind turbine rotor orientation $\delta = 60^\circ$, since at that wind turbine rotor orientation and a that equivalent pitch angle β , the U_t component is impinging perpendicularly to the maximum swept rotor area. However, blades with constant β angle produce higher straining actions than twisted blades at perpendicular positions with respect to U_t .

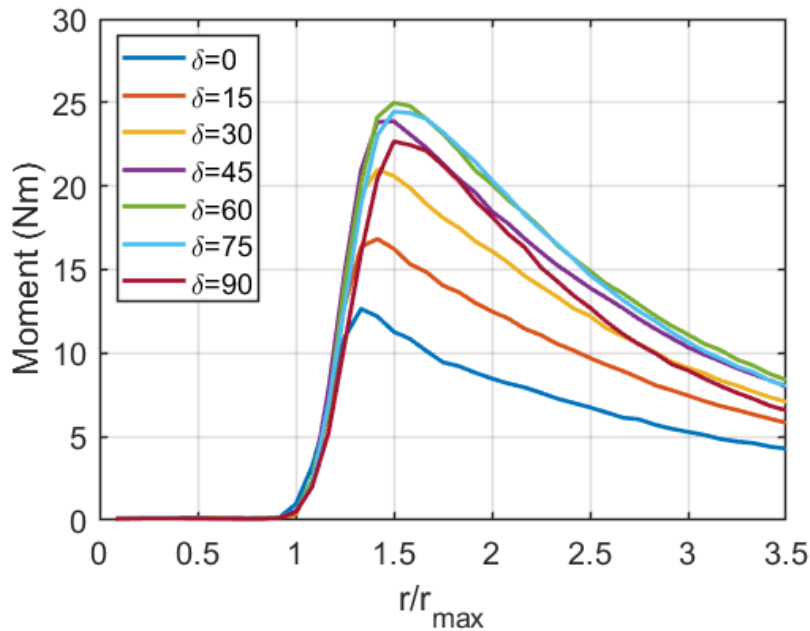


Figure 30 Overall moment on the small-scale HAWT varying delta angle and radial position

Figure 32 shows that the maximum flap-wise moment at the blade root is 3.5 times higher in Blade 1 compared to Blade 2 and 3 due to the alignment of B_1 with the vertical U_t

profile at r_{max} , which is nearly constant. In contrast, B_2 and B_3 are impacted by lower U_t velocities found outside r_{max} proximity, due to the span-wise length of the blades. For the three blades, the minimum flap-wise moment was produced when the blades are feathered, and the rotor is in the align with the stream-wise wind direction. When comparing the flap-wise moment on Blade 1 at $r/r_{max} = 1.5$, the change produced by varying β from perpendicular to feathered position is negligible when $\delta < 15^\circ$, and the maximum moment variation found at $\delta = 90^\circ$ is approx. 30%, as depicted in Figure 33.

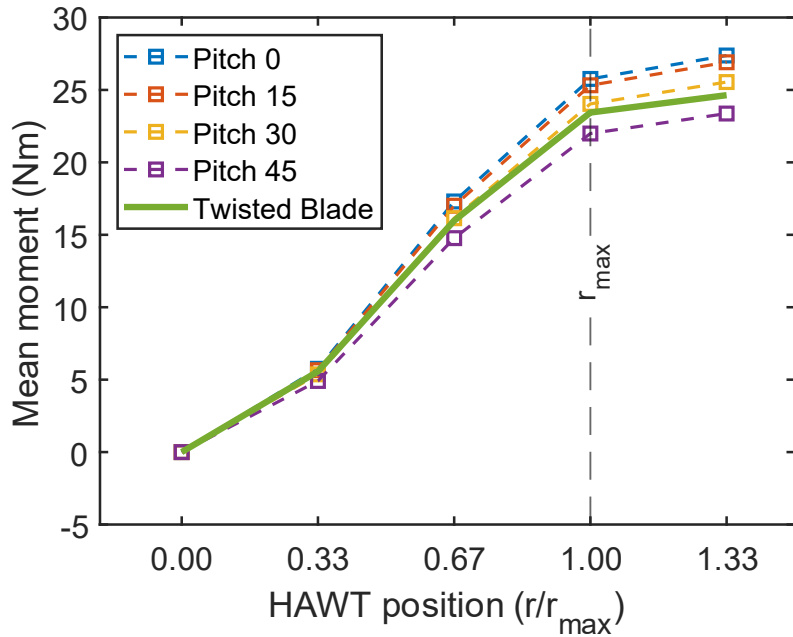


Figure 31 Comparison of the bending moment at the tower base for a HAWT with constant pitch angle and twisted blades

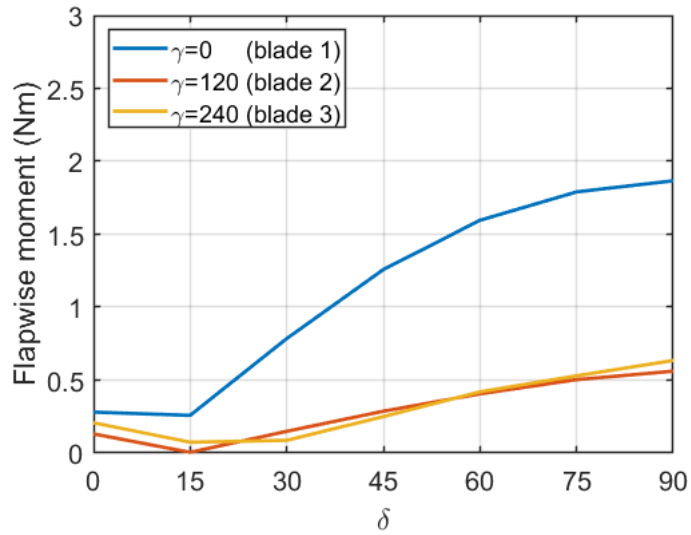


Figure 32 Flap-wise moment on the blades of the HAWT at different tornado approaching angle

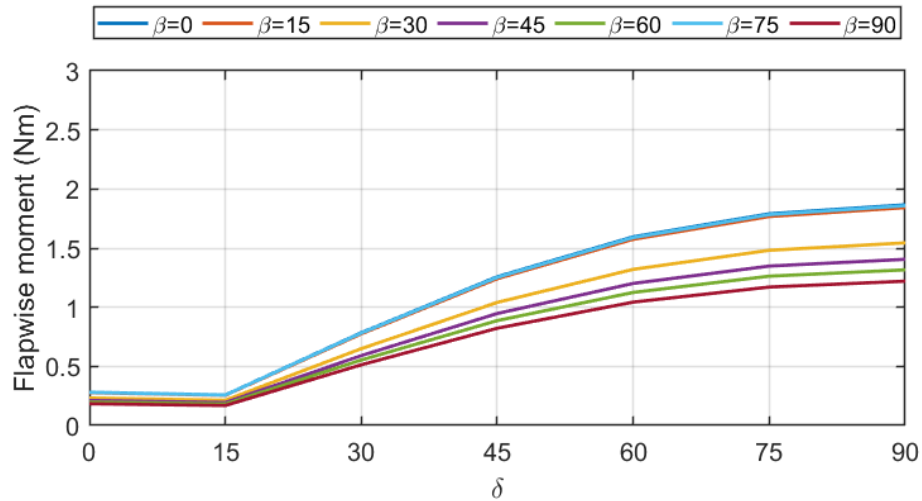


Figure 33 Flap-wise moment on the blades varying the pitch and tornado approaching angle

Figure 34 shows the overall moment at the tower base at $r/r_{max} = 1.5$ for different pitch angles and tornado approaching angles. As Figure 30 demonstrated the maximum straining actions were found when the tornado approaches at $\delta = 60^\circ$ and the twisted blades are oriented at $\beta = 0^\circ$, where their resultant forces are equivalent to those

generated from blades with constant $\beta = 30^\circ$, resulting in a rotor plane and blades oriented perpendicular to the U_t component. By varying the pitch angle β from 0° to 90° at a rotor orientation $\delta = 60^\circ$, the maximum mean moments at the tower base were reduced by 40%. However, by varying the rotor orientation δ from 60° , where the maximum mean moments at the tower base were found, to $\delta = 150^\circ$, the straining actions were reduced by 80% achieving the minimum moments at the tower base. Therefore, the optimum pitch and tornado approaching angle that leads to minimum straining actions on both the blades and the tower were found to be: $\beta = 30^\circ$ and $\delta = 150^\circ$. Consequently, the most significant active control variable of a HAWT used to reduce the response to HIW is the rotor orientation rather than the pitch angle. Orienting the rotor plane parallel to the incoming wind direction reduces the impinging area of the blade when they are feathered. Although, tornado wind fields are three-dimensional flows, it has been demonstrated that the U_t component induced loads are the most important in magnitude and variation. It may be feasible to determine the direction of the U_t component during a tornado event by tornado path prediction, wind farm measurements or based on the HAWT instrumentation, and eventually change the rotor orientation to reduce the straining actions on the system.

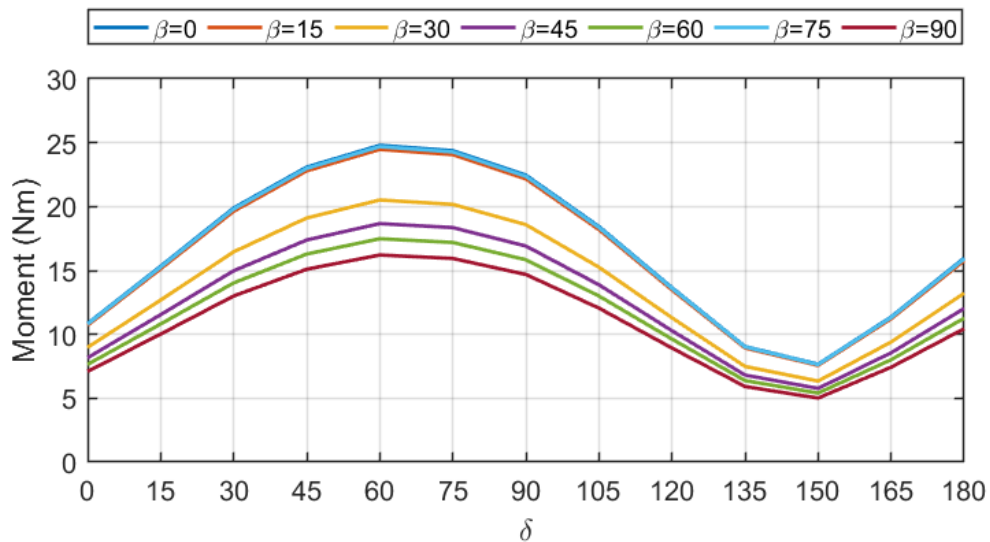


Figure 34 Moment at the base of the tower of a HAWT varying the pitch and approaching tornado angles

3.5 Conclusions

The HIW-TUR code was experimentally validated by comparing the numerical base moments M_x at the tower base with those from the experimental test obtained in the WindEEE Dome (Lopez et al., 2021). Overall, the HIW-TUR code was capable of identify the tornado location that leads to the maximum straining actions on a HAWT and the magnitude of the peak moments within an acceptable range of accuracy. By using the validated HIW-TUR, it was demonstrated that the maximum moment at the base of the HAWT were found past r/r_{max} due to the positively skewed distribution of the U_t component associated with the tornado-like vortex. The flap-wise moment on the rotor blades were fully dependent on the wind turbine rotor orientation, due to the three-dimensional nature of the tornadic flow. The highest flap-wise moment was proved to be 3.5 higher when acting on the vertical blade compared to the other two blades. This is due to the alignment of the vertical blade with the quasi constant U_t vertical velocities. It was demonstrated that the straining actions on the blades and HAWT could be reduce up to 40% by varying the pitch angle β to a feathered position with respect to U_t . Moreover, by varying the yaw angle of the rotor plane parallel to the stream-wise wind direction the moments could be reduced up to 80%. The findings in the current research could lead to recommendation for generalized guidelines for reducing the straining actions of tornado events on HAWT by active pitch and yaw control.

3.6 References

- AbuGazia, M., El Damatty, A., Dai, K., Lu, W., & Ibrahim, A. (2020). Numerical model for analysis of wind turbines under tornadoes. *Engineering structures*, 223, 111157. <https://doi.org/10.1016/j.engstruct.2020.111157>
- Ashrafi, A., Hangan H., Romanic, D., Kasab, A., & Ezami, N. (2021). Experimental investigation of large-scale tornado-like vortices. *Journal of Wind Engineering and Industrial Aerodynamics*, 208(104449). <https://doi.org/10.1016/j.jweia.2020.104449>

- Chang, C.C. (1971). Tornado wind effects on buildings and structures with laboratory simulation. *Third International Conference on Wind Effects on Buildings and Structures*, 231-240.
- Ezami, N. (2021). Behaviour of Transmission Lines Subjected to Tornadoes Through Aeroelastic Testing and Numerical Modeling. *Electronic Thesis and Dissertation Repository*, 8339. <https://ir.lib.uwo.ca/etd/8339>
- Hamada, A., El Damatty, A.A., Hangan, H., & Shehata, A.Y. (2010). Finite element modelling of transmission line structures under tornado wind loading. *Wind and Structures an International Journal*, 13(5), 451-469. <https://doi.org/10.12989/was.2010.13.5.451>
- Hamada, A., & El Damatty, A.A., (2011). Behaviour of guyed transmission line structures under tornado wind loading. *Computers & Structures*, 89(11–12), 986-1003. <https://doi.org/10.1016/j.compstruc.2011.01.015>
- Hamada, A., & El Damatty, A.A. (2015). Failure analysis of guyed transmission lines during F2 tornado event. *Engineering Structures*, 85, 11-25. <https://doi.org/10.1016/j.engstruct.2014.11.045>
- Hangan, H. (2014). The Wind Engineering Energy and Environment (WindEEE) Dome at Western University. *Wind Engineers JAWE*, 39(4), 350-351. <https://doi.org/10.5359/jawe.39.350>
- Ibrahim, A.M., El Damatty, A.A., & Elansary, A.M. (2017). Finite element modelling of pre-stressed concrete poles under downbursts and tornadoes. *Engineering Structures*, 153, 370-382. <https://doi.org/10.1016/j.engstruct.2017.10.047>
- International Renewable Energy Agency (IRENA). (2021). *Renewable capacity statistics 2021*. International Renewable Energy Agency, Abu Dhabi ISBN 978-92-9260-342-7

- Jischke, M.C., & Light, B.D. (1983). Laboratory simulation of tornadic wind loads on a rectangular model structure. *Journal of Wind Engineering and Industrial Aerodynamics*, 13(1-3), 371-382. [https://doi.org/10.1016/0167-6105\(83\)90157-5](https://doi.org/10.1016/0167-6105(83)90157-5)
- Kosiba, K., & Wurman, J. (2013). The three-dimensional structure and evolution of a tornado boundary layer. *Weather and Forecasting*, 28(6), 1552-1561. <https://doi.org/10.1175/WAF-D-13-00070.1>
- Lopez, J.P., Horia, H., & El Damatty, A.A. (2022). Experimental study of the loads induced by a large-scale tornado simulation on a HAWT model. *Wind and Structures*, 34(3), 303-312. <https://doi.org/10.12989/was.2022.34.3.303>
- Mishra, A.R., James D.L., & Letchford, C.W. (2008). Physical simulation of a single-celled tornado-like vortex, Part B: Wind loading on a cubical model. *Journal of Wind Engineering and Industrial Aerodynamics*, 96, 1258-1273. <https://doi.org/10.1016/j.jweia.2008.02.027>
- National Oceanic and Atmosphere Administration (NOAA). (2012). *May 19th, 2012, Kingman & Harper County tornadoes*. National Weather Service. https://www.weather.gov/ict/event_05192012
- Refan, M., & Hangan, H. (2012). Aerodynamic Performance of a Small Horizontal Axis Wind Turbine. *Journal of Solar Energy Engineering*, 134(2). <https://doi.org/10.1115/1.4005751>
- Sarkar, P., Sengupta, A., Haan, F.L., & Balaramudu, V. (2008). Transient loads on buildings in microburst and tornado winds. *Journal of Wind Engineering and Industrial Aerodynamics*, 96, 2173-2187. <https://doi.org/10.1016/j.jweia.2008.02.050>
- Sarkar, P., & Razavi, A. (2018). Tornado-induced wind loads on a low-rise building: Influence of swirl ratio, translation speed and building parameters.

Engineering Structures, 167, 1-12.

<https://doi.org/10.1016/j.engstruct.2018.03.020>

- Shirzadeh, K., Hangan, H., Crawford, C., & Tari, P.H. (2020). Investigating the loads and performance of a model horizontal axis wind turbine under IEC extreme operational conditions. *Wind Energy Science*, 6, 477-489.

<https://doi.org/10.5194/wes-6-477-2021>

Chapter 4

4 Conclusion

Wind energy has been demonstrated to be a reliable renewable energy alternative to reduce the usage of fossil fuels, with a significant projected growth around the world and North America in the following decades. However, in order to fulfill the profitability of new wind turbine developments, larger wind turbines must be installed in areas prone to localized High-Intensity Winds (HIW), such as tornadoes. Consequently, turbine design and control strategies should be assured to help these new systems to withstand these extreme wind conditions.

Literature review suggests that tornado-induced loads acting on different civil structures are more dangerous for wind turbines than strong synoptic winds. Moreover, there is an important absence of research regarding tornado-wind turbine interactions, and the effects of three-dimensional wind field-induced loads on the wind turbine orientation, wind turbine rotor position and condition.

The present study aimed to evaluate the tornado-induced loads acting on a wind turbine for different radial locations and rotor positions. An experimental test was carried out on a small-scale wind turbine subjected to a large-scale tornado simulation at different radial positions and rotor operation conditions. Following the laboratory measurements, an experimental validation of the numerical code HIW-TUR was carried out by comparing the experimental and numerical mean bending moments acting on the parked wind turbine. In further research, the HIW-TUR code, once validated, was employed to expand the number of variables limited by time and cost in a laboratory test. Therefore, the induced forces acting on the wind turbine and rotor blades were evaluated in order to identify the wind turbine configuration that could lead to structural failure and that could reduce the loads acting on the wind turbine and individual elements.

Results demonstrated that the straining actions on the wind turbine are dependent on the tornado distance from the wind turbine and its approaching direction. The overall bending moment is increased when the wind turbine is found in the vicinity of the

maximum radial distance. This moment acting on the wind turbine was larger than those produced by an Atmospheric Boundary Layer (ABL) flow with equivalent wind speed at the hub height, even for ABL flows defined with the extreme turbulence model (ETM) in the International Electrotechnical Commission (IEC) standard 61400-1.

The experimental validation proved that the HIW-TUR code was capable of identifying the tornado location that leads to the maximum straining actions on a HAWT and the magnitude of the peak moments within an acceptable range of accuracy. Additionally, the numerical results identified the tornado location that leads to the peak straining actions on the tower and blades for a variety of yaw and pitch angles, and those that minimized on both the blades and the tower.

4.1 Recommendation and future work

Overall, this research represents an initial assessment of experimental tornado-induced loads acting on wind turbines and the effects of the rotor positioning. Future work should include the dynamic behaviour of an aeroelastic model of HAWT under tornadoes. Large wind turbines are elastic structures, and blades should be subjected to dynamic stresses due to wind loads.

The results obtained from this research could be used in further comprehensive research with the purpose to improve the structural safety of wind turbines through control strategies during tornadoes. Rotor and blade positioning could reduce the loads acting on the wind turbine elements due to inappropriate element orientation, such as pitch and yaw angles.

Curriculum Vitae

Name: Juan Pablo Lopez Ortiz

**Post-secondary
Education and
Degrees:** University of Valley of Mexico
Villahermosa, Tabasco, Mexico
2004-2009 B.A.

Autonomous University of Yucatan
Merida, Yucatan, Mexico
2014-2016 MEdSc.

**Honours and
Awards:** Mexican National Council for Science and Technology
Scholarship
2019-2022

Publications:

Lopez, J.P., Horia, H., & El Damatty, A.A. (2022). Experimental study of the loads induced by a large-scale tornado simulation on a HAWT model. *Wind and Structures*, 34(3), 303-312. <https://doi.org/10.12989/was.2022.34.3.303>